Bioactive Materials 36 (2024) 221–237

Contents lists available at ScienceDirect

Bioactive Materials

journal homepage: www.keaipublishing.com/en/journals/bioactive-materials

Engineering an extracellular matrix-functionalized, load-bearing tendon substitute for effective repair of large-to-massive tendon defects

Shuting Huang [a,b,e], Ying Rao [a,b], Meng Zhou [a,b,d], Anna M. Blocki [a,b,d,e], Xiao Chen [f,g,h], Chunyi Wen [i], Dai Fei Elmer Ker [a,b,c,d,e], Rocky S. Tuan [a,b,e,**], Dan Michelle Wang [a,b,c,d,e,*]

[a] School of Biomedical Sciences, Faculty of Medicine, The Chinese University of Hong Kong, Hong Kong SAR, China
[b] Institute for Tissue Engineering and Regenerative Medicine, Faculty of Medicine, The Chinese University of Hong Kong, Hong Kong SAR, China
[c] Ministry of Education Key Laboratory for Regenerative Medicine, Faculty of Medicine, The Chinese University of Hong Kong, Hong Kong SAR, China
[d] Department of Orthopaedics and Traumatology, Faculty of Medicine, The Chinese University of Hong Kong, Hong Kong SAR, China
[e] Center for Neuromusculoskeletal Restorative Medicine, Hong Kong Science Park, Hong Kong SAR, China
[f] Dr. Li Dak Sum-Yip Yio Chin Center for Stem Cells and Regenerative Medicine and Department of Orthopedic Surgery of the Second Affiliated Hospital, Zhejiang University School of Medicine, Hangzhou, China
[g] Department of Sports Medicine, Zhejiang University School of Medicine, Hangzhou, China
[h] China Orthopedic Regenerative Medicine Group (CORMed), Hangzhou, China
[i] Interdisciplinary Division of Biomedical Engineering, The Hong Kong Polytechnic University, Hong Kong SAR, China

ARTICLE INFO

Keywords:
Tendon regeneration
Large-to-massive tendon defect
Tendon tissue engineering
Extracellular matrix
Polyurethane

ABSTRACT

A significant clinical challenge in large-to-massive rotator cuff tendon injuries is the need for sustaining high mechanical demands despite limited tissue regeneration, which often results in clinical repair failure with high retear rates and long-term functional deficiencies. To address this, an innovative tendon substitute named "BioTenoForce" is engineered, which uses (i) tendon extracellular matrix (tECM)'s rich biocomplexity for tendon-specific regeneration and (ii) a mechanically robust, slow degradation polyurethane elastomer to mimic native tendon's physical attributes for sustaining long-term shoulder movement. Comprehensive assessments revealed outstanding performance of BioTenoForce, characterized by robust core-shell interfacial bonding, human rotator cuff tendon-like mechanical properties, excellent suture retention, biocompatibility, and tendon differentiation of human adipose-derived stem cells. Importantly, BioTenoForce, when used as an interpositional tendon substitute, demonstrated successful integration with regenerative tissue, exhibiting remarkable efficacy in repairing large-to-massive tendon injuries in two animal models. Noteworthy outcomes include durable repair and sustained functionality with no observed breakage/rupture, accelerated recovery of rat gait performance, and >1 cm rabbit tendon regeneration with native tendon-like biomechanical attributes. The regenerated tissues showed tendon-like, wavy, aligned matrix structure, which starkly contrasts with the typical disorganized scar tissue observed after tendon injury, and was strongly correlated with tissue stiffness. Our simple yet versatile approach offers a dual-pronged, broadly applicable strategy that overcomes the limitations of poor regeneration and stringent biomechanical requirements, particularly essential for substantial defects in tendon and other load-bearing tissues.

1. Introduction

Tendons are dense fibrous connective tissue bands with high tensile strength that play a crucial role in facilitating force transmission during musculoskeletal movement [1]. However, due to their poor innate regenerative capacity, tendons are susceptible to injuries caused by acute (overload) or degenerative aging processes [2]. Substantial tendon injuries, such as large rotator cuff tears (RCTs), present significant challenges for shoulder surgeons in clinical practice [3]. Despite clinical interventions, the failure rate remains considerably high, ranging from

Peer review under responsibility of KeAi Communications Co., Ltd.
* Corresponding author. School of Biomedical Sciences, Faculty of Medicine, The Chinese University of Hong Kong, Hong Kong SAR, China.
** Corresponding author. School of Biomedical Sciences, Faculty of Medicine, The Chinese University of Hong Kong, Hong Kong SAR, China.
E-mail addresses: tuanr@cuhk.edu.hk (R.S. Tuan), wangmd@cuhk.edu.hk (D.M. Wang).

https://doi.org/10.1016/j.bioactmat.2024.02.032
Received 8 January 2024; Received in revised form 22 February 2024; Accepted 23 February 2024

20 to 90% [4,5]. This high failure rate can be attributed to incomplete healing and the formation of fibrovascular scar tissue, which compromises the mechanical properties of the repaired tendon with the Young's modulus compromised by up to 60% compared to normal tendons, especially in cases of large-to-massive tendon tears [6–8]. Therefore, it becomes crucial to deliver highly robust tissue-specific regenerative cues along with adequate mechanical competence to support tendon functional movement for successful tendon repair, particularly in cases of large-to-massive tendon defects [9–11].

After injury, tendons typically demonstrate a reparative response rather than regenerative healing, which is characterized by scar formation with disorganized extracellular matrix (ECM) that could not sustain significant tensile forces [11,12]. Consequently, achieving functional tendon repair necessitates biological augmentation to recapitulate native tendon-like tissue structure. This includes well-organized, aligned tendon ECM, as the fiber alignment significantly correlates with tendon's mechanical parameters, enabling it to bear tensile forces and prevent re-tears after repair [13]. Current state-of-the-art research efforts have attempted to apply various methods to enhance the biological response of tendons (*e.g.*, cell chemotaxis, proliferation, matrix synthesis, and cell differentiation) *via* administration of bioactive molecules (*e.g.*, tendon-promoting growth factors (Fibroblast Growth Factor (FGF), Platelet Derived Growth Factor (PDGF), Transforming Growth Factor Beta (TGF-β), Vascular Endothelial Growth Factor (VEGF), Bone Morphogenetic Proteins (BMP), and Insulin-like Growth Factor 1 (IGF-1)), Platelet-Rich Plasmas (PRPs), Extracellular vehicles (EVs), and extracellular matrix (ECMs)) [14,15]. Among them, ECM stands out as a complex three-dimensional (3D) network of interacting macromolecules. ECM exhibits unique tissue-specific regenerative bioactivity, which sets it apart from single/combined growth factors, although potent, their use may result in unwanted, off-target ossification [16,17]. Therefore, ECM-based biomaterials have been utilized in a variety of preclinical and clinical scenarios, including several Food and Drug Administration (FDA)-approved ECM scaffolds, such as GraftJacket®, Zimmer® Collagen Repair Patch/Permacol™, and TissueMend, for clinical tendon repair [14,18,19]. Indeed, direct decellularization of tendon tissues has been used as a scaffold material to promote tendon regeneration [14]; however, the dense collagenous architecture can impede cell infiltration, with cell regeneration limited to the tissue surface [20]. To overcome these limitations while maintaining the tissue-specific bioactivity of the ECM, decellularized tissues can be solubilized with enzymatic or chaotropic agents, resulting in a solution form that can be combined with a diverse array of biomaterials [14].

Furthermore, mechanical augmentation is another critical aspect of achieving functional tendon regeneration, particularly in case of large tendon injuries [21]. By utilizing grafts with properties resembling those of natural tissue, it becomes possible to restore shoulder movement to pre-injury levels while minimizing the risk of repair construct failure, enabling the tendon to complete its lengthy healing process. Consequently, various tendon substitute/scaffolds have been developed to provide mechanical augmentation for tendon repair [22]. These include degradable biomaterials such as polycaprolactone (PCL), polylactic acid (PLA), and poly(L-lactide) (PLLA), as well as nondegradable materials like polyethylene terephthalate (PET) patch [23,24]. Despite these diverse approaches, a singular approach has yet to achieve complete functional repair and regeneration. The mismatched structural and/or mechanical properties compared to native tendons presumably contributes to high re-tear rates in large-to-massive tendon injuries [19]. Additionally, current ECM scaffolds, despite their potent bioactivity, often display huge disparities between their structural and material properties and those of tendons. This suggests that these scaffolds may not provide sufficient mechanical reinforcement to primary rotator cuff repair [18]. As such, mechanical augmentation of ECM-based scaffolds is a critical approach to improve their clinical performance for tendon repair. For instance, combining ECM with synthetic biomaterials may be expected to yield a synergetic effect between natural and synthetic polymers [18]. Recent efforts have included embedding collagen-glycosaminoglycan scaffolds with 3D-printed synthetic acrylonitrile butadiene styrene polymers [25], electrochemical alignment of collagen to produce mechanically-strong ECM-based scaffolds [26], and collagen gel incorporating to a nondegradable PET filaments [27], These approaches have attained ultimate stresses (0.9 MPa) [25] and ultimate loads (59.9 N) [26], that approach those of native tendons (human supraspinatus tendon (SSPT), the most frequently torn rotator cuff tendon; ultimate stresses: 11.9–22.1 MPa [28]; ultimate load: 652 N) [29]. However, there are few reports of animal studies utilizing large-to-massive tendon defects that have achieved similar mechanical attributes as native intact tendon.

To biologically augment tendon regenerative capacity, our group has developed a bioinspired strategy of using the ECM's rich biocomplexity for tissue-specific regeneration *via* our unique urea-based protocol for collecting soluble, DNA-free, tendon ECM extracts (tECM) [30–32]. Compared to other approaches that have been widely used in research or clinical practice, urea-extracted tECM is markedly distinct [32,33]. Traditional acid pepsin extraction lacks sufficient non-collagenous matrix [34], while single/combined growth factors, although potent, may result in unwanted, off-target bone/cartilage formation [35]. Also, other tissue-derived ECM such as skin-based scaffolds have limited reports of tendon-specific bioactivity [36]. In contrast, our previous research has shown that tECM retains a substantial number of non-collagenous tendon ECM components that are critical for tendon development and regeneration. It induces unique transcriptomic profiles compared to collagens, and exhibits tissue-specific regenerative bioactivity on stem cells [32,33].

To mechanically support tendon repair, our group has also developed a UV-crosslinkable polyurethane elastomer (*i.e.*, QHM), which is formulated with quadrol (Q), hexamethylene diisocyanate (H), and methacrylic anhydride (M), and is free of solvent, catalyst, and photoinitiator [37]. As shown, QHM exhibits human SSPT-like biomechanical properties, excellent suture retention *ex vivo*, slow degradation profiles with low cytotoxicity *in vitro*, and good biocompatibility *in vivo* [37]. Critical considerations in engineering biomaterials for rotator cuff repair include tendon-like mechanical properties to support physiological loading and biophysiochemical attributes that stabilize the repair site over the long-term [38]. Thus, these superior features of QHM elastomer make it highly feasible to provide long-term mechanical support that matches the lengthy tendon healing process.

Expanding on our prior work, we aim to simultaneously achieve robust tendon regeneration and adequate mechanical support by developing a bioactive hybrid scaffold, called BioTenoForce. This scaffold will feature a core-shell structure that assembles the tECM-enriched gelatin methacryloyl (GelMA) hydrogel and mechanically robust QHM through covalent crosslinking. To investigate the healing efficacy of BioTenoForce for tendon repair, a comprehensive series of assessments was performed, including: (i) systematic characterization of BioTenoForce components, including the biomechanical properties of the elastomer core, tECM composition and tenogenic bioactivity, as well as hydrogel degradation and tECM release kinetics; (ii) *ex vivo* characterization of BioTenoForce bonding robustness, mechanical properties, and suture retention capabilities; (iii) *in vitro* tenogenic differentiation of human adipose-derived stem cells (hASCs) encapsulated in BioTenoForce; and (iv) *in vivo* evaluation of BioTenoForce biocompatibility (using a mouse subcutaneous implantation model) and tendon healing efficacy (using a rat large rotator cuff tendon defect model and a rabbit massive rotator cuff tendon defect model) (Scheme 1).

2. Methods and materials

2.1. Study design

To address the challenging issue of repairing large-to-massive rotator

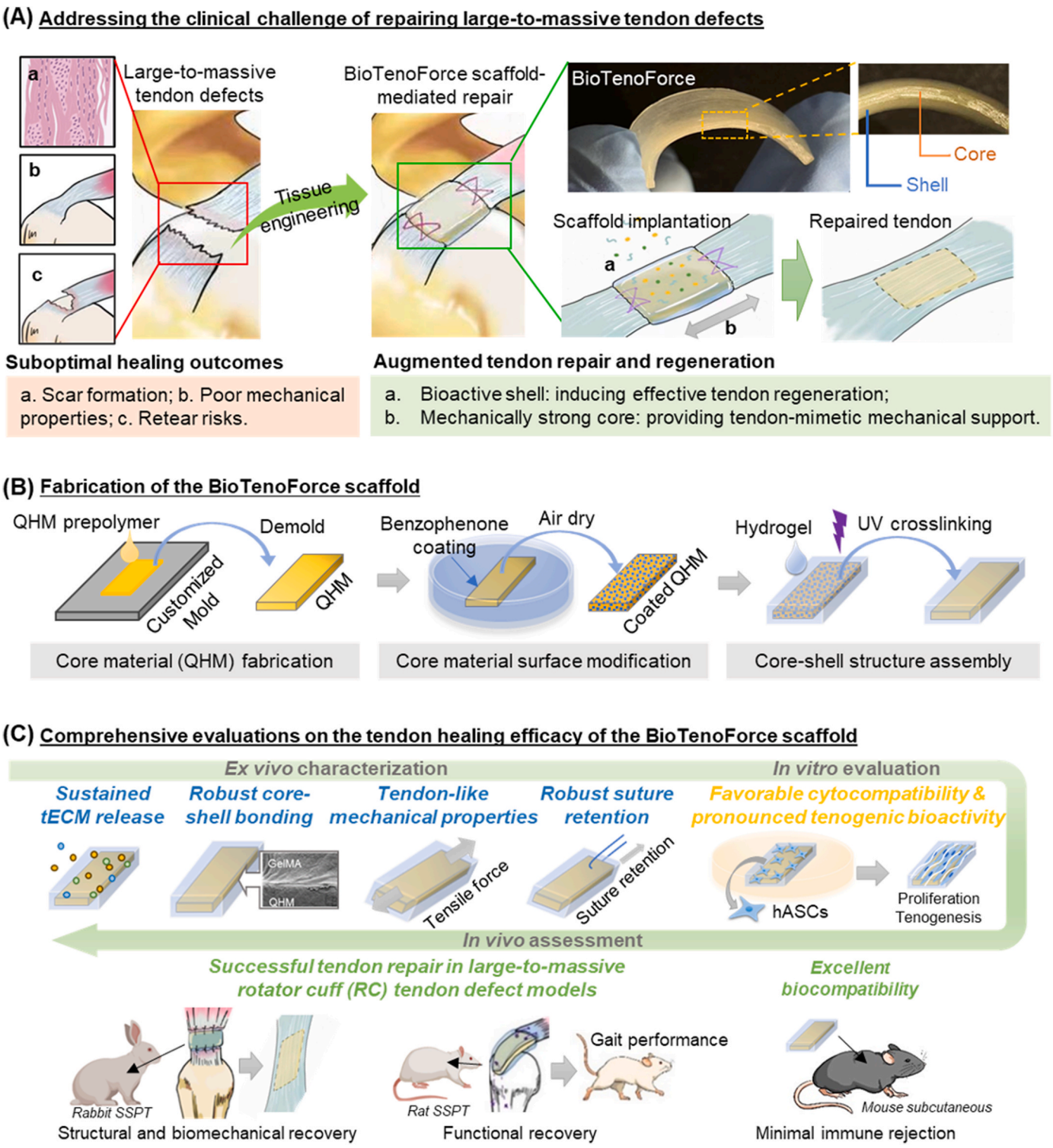

Scheme 1. Study overview of BioTenoForce development and characterization. (A) The clinical challenges of repairing large-to-massive tendon defects and the concept of our BioTenoForce scaffold design. **(B)** The core portion (QHM elastomer, as a mechanically robust scaffold component) of BioTenoForce is bonded to a shell portion (tECM hydrogel, supplementing tenogenic cues) using benzophenone-mediated photocrosslinking. **(C)** A series of comprehensive evaluations was performed to determine the suitability of BioTenoForce for clinical translation in the repair of large-to-massive tendon defects.

cuff tendon defects, we developed a core-shell structured hybrid construct, called BioTenoForce, and conducted a vigorous characterization to assess its suitability for clinical translation. We started with systematic characterization of the scaffold constituent components to ensure its production and characteristics were reproducible before manufacturing. Subsequently, we evaluated the bonding robustness, mechanical properties, and suture retention capabilities of BioTenoForce, which are essential for rotator cuff repair stability. Later, we investigated the tenogenic bioactivity of BioTenoForce on hASCs *in vitro*, as well as its biocompatibility using a mouse subcutaneous implantation model. Finally, we evaluated the efficacy of BioTenoForce in tendon healing for repairing large-to-massive rotator cuff defects in both rats

and rabbits by assessing the functional (gait analysis), structural (histology analysis, SEM), and biomechanical (nanoindentation and bulk tensile test) aspects. All data points collected were included in the analysis of experiments, and no outliers were excluded. All experiments were randomized and blinded where possible. For *ex vivo* assays, a minimum of three independent experiments were performed, unless otherwise noted. For *in vitro* and *in vivo* assays, experiments were performed with at least three biological repeats per group. For animal experiments, animals with similar age, weight were grouped randomly.

2.2. Isolation and characterization of hASCs

To obtain hASCs, cells were isolated from the infrapatellar fat pad tissue from patients (4 donors, 59–74 years old, male and female) undergoing total knee replacement surgery. The isolation procedure followed the guidelines and received approval from the Institutional Review Board approval as previously described [31]. The isolated cells were further sorted using a human mesenchymal stem cells (hMSC) analysis kit (BD Biosciences; positive markers including CD90, CD105, CD73, and CD44; negative markers including CD34, CD11b, CD19, CD45, and HLA-DR). The cells were then subjected to colony-forming unit-fibroblast (CFU–F) and tri-lineage differentiation assays until passage 7 as previously described [31]. Only hASCs from passages 2–5 were used in the present study.

2.3. BioTenoForce fabrication process

To fabricate the BioTenoForce, we developed a straightforward method for assembling preshaped QHM elastomer and tECM-containing GelMA hydrogel into a core-shell structured hybrid construct. The three major components included in BioTenoForce fabrication are tECM, GelMA hydrogel, and QHM elastomer. To obtain soluble tECM extracts, bovine Achilles tendon from adult bovines was purchased from a commercial market (Hong Kong) and subjected to urea-based extraction as described previously [31]. To prepare GelMA prepolymer solution, 10% GelMA (EFL) with or without tECM (final concentration in hydrogel: 0.6 mg/mL, by bicinchoninic acid (BCA) assay, was dissolved in PBS with 0.25% (w/v) photoinitiator (lithium acylphospinate salt, LAP; EFL). A UV-crosslinkable polyurethane elastomer, QHM, was developed based on our published protocol [37] with minor modification of including an extra drying step for Q. Briefly, to develop BioTenoForce, the surface of the QHM elastomer was treated by absorbing benzophenone as described previously [39]. Thereafter, the GelMA prepolymer solution was gently applied onto the freshly treated QHM and exposed to UV irradiation using a UV lamp (EFL; 365 nm, 25 mW/cm^2) for 90 s.

Furthermore, several procedures were performed to ensure consistent quality standards of BioTenoForce and avoid batch to batch variations, including: (1) tECM characterization: dsDNA assay, hydroxyproline assay, sulfated proteoglycans and sulfated glycosaminoglycan (sGAG) assay, and SDS-PAGE were performed to assess tECM decellularization, collagen content, sGAG content, and protein composition, respectively; (2) tECM bioactivity analysis: The tenogenic bioactivity of tECM from each batch of extraction was characterized on hASCs in 2D culture *via* established markers (SCX, MKX, TNC, and COL1) *via* qPCR and immunofluorescence staining as described previously [31]; (3) GelMA hydrogel: Swelling assay, degradation study, tECM release assay were performed to determine hydrogel swelling behavior, degradation properties, and tECM protein release profile, respectively; and (4) QHM elastomer: Tensile test was conducted on the QHM elastomer to examine its biomechanical properties and ensure that these properties are comparable with our reported data [37]. A detailed description can be found in the supplementary materials.

2.4. Characterization of the interfacial bonding strength, mechanical properties, and suture retention value of BioTenoForce

A series of experiments were conducted to comprehensively evaluate the interfacial bonding strength, mechanical properties, and suture retention value of BioTenoForce. Firstly, the interfacial bonding strength between the GelMA hydrogel (rectangular shape; 5 mm width × 30 mm length × 1 mm thickness) and QHM elastomer (rectangular shape; 30 mm width × 50 mm length × 5 mm thickness) by a standard 90-degree peeling test according to the guidelines in the ASTM 6862 with a peeling rate of 50 mm/min [39]. The cross-sectional interface of BioTenoForce was also characterized by SEM (Hitachi SU8010). Additionally, to test the bonding robustness *in vivo*, BioTenoForce (a round disk shape; 8 mm diameter × 2 mm thickness) was subcutaneously implanted to mice. At designated time points (post-surgery days 7 and 18), scaffolds and surrounding tissues were harvested for histological analysis. To ensure that the surface coating and crosslinking procedure would not largely modify the mechanical properties of the QHM elastomer, tensile and suture retention tests were performed to compare the biomechanical properties of BioTenoForce with those of QHM elastomer, GelMA, and ADM (Wright Medical). Tensile test was conducted on samples fabricated in a mini type IV shape (proportionally shrink for 3.2 times from original size) according to the guidelines in the ASTM D638-10. A horizontal mechanical tester (Admet) equipped with a 500 lb load cell was used together with MTestQuattro software (Admet, Version 6.00.05) to acquire tensile data. Tensile stress or strain at yield was defined as tensile stress or strain at which samples yielded (slope where the stress–strain curve equals zero), respectively. Ultimate strength or strain was defined as the maximum strength or strain at which samples failed, respectively. Tensile modulus was defined as the initial linear slope of the stress–-strain curve and calculated from 0% to 0.5% strain. Suture retention test was performed on samples prepared and tested as shown in Fig. 3B. A horizontal mechanical tester (Admet, a 100 lb load cell) was used together with MTestQuattro software (Admet, Version 6.00.05) to acquire data.

2.5. Evaluation of cytocompatibility and tenogenic effect of BioTenoForce in vitro

hASCs were encapsulated in the gel layer of TenoForce or BioTenoForce, and a set of experiments were performed to characterize cell viability, proliferation, and tenogenic differentiation. In brief, hASCs (passage 2–5, 4 million/mL) were mixed with GelMA prepolymer containing either 20% (v/v) tECM (final concentration in gel: 0.6 mg/mL) as BioTenoForce group or 20% (v/v) PBS as TenoForce group to formed hybrid constructs by UV irradiation (365 nm, 25 mW/cm^2, 90 s). Different groups of scaffolds were cultured in growth medium (DMEM-high glucose (Thermo Fisher), 10% (v/v) FBS, 1% (v/v) Penicillin/Streptomycin, and 50 ng/mL ascorbic acid (Santa Cruz)). On designated time points (*i.e.*, days 0, 7, 10, and 14), Live/Dead (Invitrogen) and dsDNA (Quant-iT PicoGreen dsDNA Reagent, Invitrogen) assays were performed to determine cell viability and dsDNA content, respectively. To evaluate hASC tenogenic differentiation, tenogenesis-associated markers (*SCX, MKX, TNC, and COL1A1*) were assessed *via* qPCR and (TNC, COL1, TNMD, and F-actin) *via* fluorescence staining as previously described [31]. A detailed description can be found in the supplementary materials.

2.6. Evaluation of histocompatibility of TenoForce and BioTenoForce in a mouse subcutaneous implantation model

Histological examinations were performed to investigate scaffold histocompatibility using a mouse subcutaneous implantation model, following approved guidelines from the institution's Animal Experimentation Ethics Committee (Ref. No. 21-170-MIS). Each mouse was implanted with one TenoForce and one BioTenoForce scaffolds in a

round disk shape (8 mm diameter × 2 mm thickness) and euthanized at designated time points (post-surgery days 7 and 28) for further histological examination. H&E staining was performed to evaluate tissue morphology and cellular infiltration while immunohistochemical staining was performed to detect macrophages (CD11b, Abcam). Images were captured using an upright microscope (Nikon). A detailed description can be found in the supplementary materials.

2.7. Evaluation of shoulder functional recovery using gait analysis in a rat large tendon defect model

Restoring shoulder function is crucial for patients with rotator cuff tears [40]. Therefore, to assess tendon functional repair mediated by BioTenoForce, a large rotator cuff tendon defect (removing a 1-mm length of tendon, full thickness tear) was created in the rat SSPT (healthy rat SSPT is around 3.5 mm in length [41]) according to previously published studies [42,43], in accordance with the approved guidelines of the institution's Animal Experimentation Ethics Committee (Ref. No. 19-266-MIS). A total of 36 Sprague-Dawley rats (gender: male; average age: 12 weeks; weight, 250g; Laboratory Animal Services Centre (LASEC), The Chinese University of Hong Kong (CUHK)) were divided into 3 groups (n = 12 per group): (1) the intact control group, (2) defect only group, and (3) BioTenoForce implantation group. For the intact control group, no defect or treatment was performed. Prior to the surgery, rats were weighted and then anesthetized with a mixture of ketamine (75 mg/kg, i.p.) and xylazine (10 mg/kg, i.p.). For the defect only group, no treatment was applied after creating the tendon defects and the wound was closed immediately after the surgery. For the BioTenoForce implantation group, a 5.0 Prolene suture (Ethicon) was passed through the SSPT and firmly secured on to the scaffold (rectangle shape; 2 mm width × 3 mm length × 1 mm thickness) using a modified Mason-Allen technique [43–45]. Another suture end was passed through the bone tunnels, which were drilled at the greater tuberosity using a 0.5 mm drill, and tied with the scaffold approximated to the anatomic footprint on the greater tuberosity [42]. Gait analysis was conducted 2 days before surgery as well as 14 days, 28 days, and 56 days after surgery, and an automated Catwalk system (Catwalk XT 9.0; Noldus) with motorized platform microscope (Leica) and ImagePro image premier analysis software (Media Cybernetics) were employed. The rats were pretrained to cross the walkway daily for 2 days before the surgery and data were collected to assess the presurgery gait performance. At 14, 28, and 56 days post-surgery, the walking behaviors of the rats were recorded. During data collection, the walkway was set as a horizontal platform, the camera was set at 60 cm from the walkway, and the entire run was recorded with a video camera. Recorded runs with a steady walking speed were accepted as compliant runs for paw-print autoclassification of left forelimb (LF), right forelimb (RF), left hind limb (LH) and right hind limb (RH) by the built-in software (Fig. S6). The footprint intensity, footprint area, print width, stride length, and LII were calculated [40,46].

2.8. Evaluation of repair efficacy of BioTenoForce in a rabbit massive tendon defect model

To investigate the healing efficacy of BioTenoForce for tendon tears, a rabbit massive rotator cuff tendon defect model (5 mm segmental defect with 10 mm segmental gap) was established in accordance with approved guidelines of the institution's Animal Experimentation Ethics Committee (Ref. No. 18-003-MIS). A total of 32 New Zealand White rabbits (gender: male or female; average age: 16 weeks; weight: 3.0–4.0 kg; LASEC, CUHK) were randomly assigned into 3 groups (n = 16 per group): (1) intact control group, (2) TenoForce implantation group, and (3) BioTenoForce implantation group. All animals underwent an index procedure in which either the left or right SSPT was randomly detached, with the contralateral intact shoulder serving as an intact control group. Prior to the surgery, rabbits were anesthetized with the mixture of ketamine (35 mg/kg) and xylazine (5 mg/kg) by intramuscular injection. The SSPT of rabbits was exposed by releasing parts of the trapezius and deltoid muscles through a longitudinal incision made over the shoulder. A 5 mm rectangular segmental defect (5 mm length × 10 mm width) was created by fully removing a 5 mm × 10 mm segment of the SSPT [47]. To reduce the detrimental effects of high tension repair, a 10 mm rectangular segmental gap was introduced by implanting either BioTenoForce or TenoForce scaffolds (10 mm width × 10 mm length × 2 mm thickness), which repaired in an interpositional fashion by joining each end of the scaffold with the tendon defect margin using a combination of running-locking and modified Mason-Allen suture technique [44,45,48]. The length of the suture area on the tendon was determined to be 5 mm. After implantation, the surgical wound was closed, the rabbits were euthanized by an intraperitoneal injection for pentobarbital overdose (>60 mg/kg) at the designated time points, and the entire supraspinatus muscle and tendon unit was harvested for further analysis.

To investigate the tendon healing outcomes, a series of experiments were performed, including: histological evaluation, including H&E and picrosirius red staining with polarized light microscopy; SEM for characterization of fiber orientation and thickness; nanoindentation and tensile test for evaluation of tendon biomechanical properties at micro- and macro-scales. A detailed description can be found in the supplementary materials.

2.9. Statistical analysis

All of the studies were evaluated with n ≥ 3 per group at each data point to ensure reproducibility. Sample sizes are noted in figure legends. All statistical analyses were performed using Prism 6. Student's *t*-test were used for analyzing peeling force, peak load, Live/Dead assay, dsDNA assay, and qPCR assay. Fisher's exact test were used for analyzing failure mode between bonded and nonbonded BioTenoForce. Pearson product-moment correlation coefficient was used for evaluating the relationship among fiber alignment (mean), ultimate load (medium), and stiffness (medium). Spearman's rank correlation coefficient was used for evaluating the relationship among fiber thickness (mean), fiber alignment (mean), ultimate load (medium), and stiffness (medium). One-way ANOVA followed by Tukey's post hoc test were used for the rest of the studies. All correlation coefficients (Quinnipiac University) were interpreted as follows: +1 and −1 as perfect, +0.7 to + 0.9 and −0.7 to - 0.9 as very strong, +0.4 to + 0.6 and −0.4 to −0.6 as strong, +0.3 and −0.3 as moderate, +0.2 and −0.2 as weak, +0.1 and −0.1 as negligible, 0 as none [49]. Statistically significant differences are indicated by asterisks (*, $p < 0.05$; **, $p < 0.01$; and ***, $p < 0.001$).

3. Results

3.1. Development of a core-shell structured BioTenoForce

Before manufacturing BioTenoForce, we systematically characterized its constituent components, which includes: QHM biomechanical property characterization; tECM compositions and tenogenic bioactivity test; and tECM-GelMA hydrogel swelling property, degradation, and tECM release tests *ex vivo*, as shown in Figs. S1–3. Our well-established standardized protocol has consistently yielded bioactive tECM extracts with reliable and reproducible extraction outcomes (Fig. S1). It is also important to note that we have developed a new protocol for QHM fabrication. This revised protocol includes an additional drying step for Q compared to our published protocols for QHM fabrication [37]. Specifically, tensile modulus of the QHM with the additional drying step (603.1 ± 35.3 MPa) closely approximated that of human SSPT (217.7 MPa for anterior sub-region; 592.4 MPa for posterior sub-region), whereas the QHM without the drying step (65.0 ± 7.3 MPa) did not exhibit a similar resemblance (Fig. S2) [37]. We speculate that this is because the hydroxyl group of Q reacted poorly with the isocyanate

groups of H or the anhydride group of M due to the presence of water molecules in the local humid air. Subsequent characterization of tECM-GelMA hydrogel showed that it exhibited limited swelling capacity (4.4% swelling ratio), degradability (25.7% of weight loss after 21 days), and initiated a burst release of tECM within the first 2 days followed by a sustained release profile over a period of 15 days (Fig. S3). Overall, materials that used to fabricate BioTenoForce are all systematically characterized to ensure its production and characteristics are reproducible before downstream characterization.

3.2. The core-shell structured BioTenoForce demonstrated robust interfacial bonding

The bonding integrity of a hybrid construct is essential for its successful *in vivo* application. Delamination between the core and shell structure during the early stages of tendon healing would impede our intention to simultaneously provide bioactive factors and mechanical support. The interfacial bonding strength was first assessed by analyzing the force-displacement profile and failure mode analysis (Fig. 1A). Our results showed that bonded BioTenoForce yielded significantly higher peeling force and peak load compared to nonbonded scaffold (Fig. 1A). In bonded BioTenoForce, failure occurred within the GelMA hydrogel bulk rather than at the GelMA hydrogel-QHM interface as shown by the residual layer of GelMA hydrogel remaining on the QHM elastomer (Fig. 1A). In contrast, failure of nonbonded BioTenoForce occurred at the GelMA hydrogel-QHM interface rather than within the GelMA hydrogel bulk, with the hydrogel being easily peeled off from the QHM elastomer surface (Fig. 1A). To qualitatively assess interfacial bonding integrity, scanning electron microscopy (SEM) and *in vivo* mouse subcutaneous implantation studies were performed (Fig. 1B and C). Representative SEM images showed that the GelMA hydrogel was firmly attached to the QHM elastomer in bonded BioTenoForce, while nonbonded scaffold exhibited clear delamination with little-to-no residual GelMA hydrogel on the QHM elastomer (Fig. 1B). Additionally, *in vivo* results showed that degradation of GelMA was observed at 7- and 18-days post-surgery (Fig. 1C), and the remaining hydrogel was attached to the surface of the QHM elastomer, indicating that robust bonding could be maintained *in vivo* (Fig. 1C). Overall, our results demonstrated that benzophenone-mediated photocrosslinking treatment produce bonded BioTenoForce with strong interfacial attachment strength between its hydrogel and elastomer layers.

3.3. BioTenoForce exhibited human tendon-like tensile properties and strong suture retention values

To achieve successful tendon repair in cases of large tendon defects, two critical biomechanical features for tendon substitutes are the ability to mimic native tendon mechanical properties and provide sufficient suture retention strength to prevent post-implantation suture pull-out. These features are essential to sustain tendon functional movement and ensure the long-term stability and integration of the repaired tendon. Therefore, tensile and suture retention tests were performed to confirm that benzophenone-mediated photocrosslinking during BioTenoForce fabrication does not negatively impact scaffold mechanical properties (Fig. 2). Representative force-displacement profiles showed that both the QHM elastomer and BioTenoForce exhibited an initial steep increase in load-displacement, followed by sustained plastic behavior before failure. In contrast, the commercially available acellular human dermal matrix (ADM as a clinical scaffold control) displayed a gradual increase in load-displacement, culminating in failure after sustained deformation (Fig. 2A). The stress at yield, strain at yield, tensile modulus, ultimate strength, ultimate strain, and stiffness of the QHM elastomer and BioTenoForce were similar (Fig. 2A). Notably, the QHM elastomer and BioTenoForce demonstrated human SSPT-like tensile moduli (approximately 500–600 MPa) [37], which were 400-fold higher than that of ADM and 25-thousand-fold higher than GelMA hydrogel. In suture retention test, when a 25 N force was applied, neither the QHM elastomer nor BioTenoForce exhibited any significant suture migration (less than 0.1 mm) or scaffold deformation, whereas ADM displayed substantial elongation and approximately 1.72 mm suture migration (Fig. 2B), which were around 30-fold higher. Overall, these results indicate that BioTenoForce possesses human SSPT-like tensile properties and superior suture retention properties compared to a leading commercial scaffold ADM, which are essential for rotator cuff repair stability.

3.4. hASCs encapsulated in BioTenoForce exhibited strong proliferation and tenogenic differentiation

The incorporation of tECM is intended to impart tenogenic bioactivity to the BioTenoForce. Consequently, *in vitro* evaluations were performed to investigate the effectiveness of tECM bioactivity within the scaffold and to assess whether benzophenone-mediated photocrosslinking treatment may impact tECM bioactivity. hASCs were encapsulated in the gel layer of BioTenoForce or the scaffold without tECM supplementation (called TenoForce scaffold), and a set of experiments were performed to characterize cell viability, proliferation, and tenogenic differentiation (Fig. 3A, S4-5). Live/Dead assay showed that from day 7 to day 14, both TenoForce and BioTenoForce exhibited high cell viability (more than 90%). A significantly higher amount of double stranded DNA (dsDNA) in the BioTenoForce group was detected than that in the TenoForce group after 14 days of culture (Fig. 3A). After 10 and 14 days of culture, significantly increased expression of *SCX* (Scleraxis), *MKX* (Mohawk), *TNC* (Tenascin C), and *COL1A1* (Type I collagen) was observed in the BioTenoForce relative to the TenoForce control groups (Fig. 3A). Consistently, immunofluorescence staining results showed enhanced expression of all tenogenesis associated markers (COL1, TNC, and TNMD (Tenomodulin)) in the BioTenoForce group relative to the TenoForce group (Fig. 3A). Taken together, these findings suggest that benzophenone-mediated photocrosslinking procedure did not affect BioTenoForce bioactivity. Moreover, BioTenoForce exhibited excellent cytocompatibility and markedly promoted hASC proliferation and tenogenic differentiation *in vitro* compared to TenoForce.

3.5. BioTenoForce exhibited biocompatibility in a mouse subcutaneous implantation model

To preliminarily assess the biocompatibility of BioTenoForce *in vivo*, disks of BioTenoForce and TenoForce were subcutaneously implanted into wild-type mice for histological evaluation at designated timepoints (Fig. 3B). No signs of severe inflammatory response or mortality were observed during the entire post-surgery follow-up period. At day 7, a small number of CD11b+ (a pan-myeloid marker) cells were observed at the surface area of the BioTenoForce. By day 28, both TenoForce and BioTenoForce were surrounded by a thin fibrous capsule, and there was no obvious evidence of an overexuberant inflammatory response in either implantation group. These results suggest that both TenoForce and BioTenoForce are sufficiently biocompatible.

3.6. BioTenoForce promoted fast recovery of gait performance in rats with large rotator cuff tendon defects

The recovery of tendon function is a crucial demand of patients with tendon injuries. The implantation of the BioTenoForce offers immediate mechanical support for the injured tendon while simultaneously stimulating tissue regeneration. This synergistic effect holds the potential to accelerate tendon functional recovery. Therefore, the ability of BioTenoForce to promote shoulder functional restoration was evaluated using gait analysis in a rat large rotator cuff tendon defect model (Fig. 4A–S6). Typically, rats with shoulder impairment and pain due to tendon tears avoid bearing weight on the affected paws, resulting in

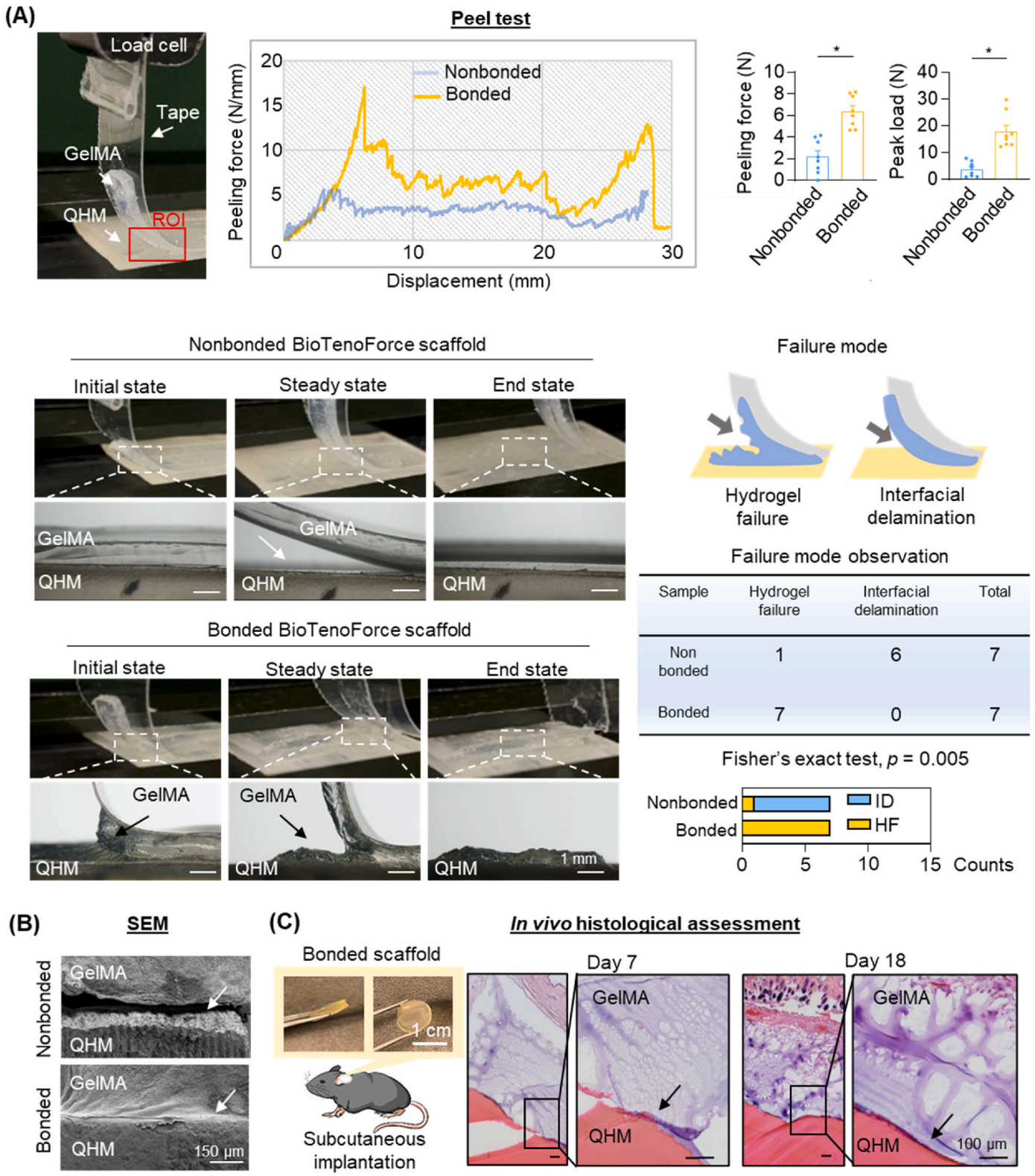

Fig. 1. ***Ex vivo*** **and** ***in vivo*** **assessment of BioTenoForce interface bonding. (A)** 90°-Peeling test: Schematic illustration showing implementation of the 90°-peeling test in accordance with American Society for Testing and Materials (ASTM) standard 6862. These results showed that bonded BioTenoForce presented a higher peeling force and peak load compared to nonbonded BioTenoForce. ROI: region of interest; HF: hydrogel failure; ID: interfacial delamination. n = 7, technical replicates; mean ± SEM; *, $p < 0.05$. **(B)** SEM analysis: Representative SEM of the cross-sectional images of the bonded and nonbonded BioTenoForce showed that GelMA hydrogel was firmly attached to the QHM elastomer after photocrosslinking treatment in bonded scaffold. White arrows indicate the interface of the GelMA hydrogel and QHM elastomer. SEM: scanning electron microscopy; n = 3, technical replicates. **(C)** Subcutaneous implantation study: Histological analysis at 7- and 18-days post-surgery demonstrated the interface attachment between GelMA and QHM elastomer in the bonded BioTenoForce. Black arrows indicate the interface of the GelMA hydrogel and QHM elastomer. n = 3, biological replicates.

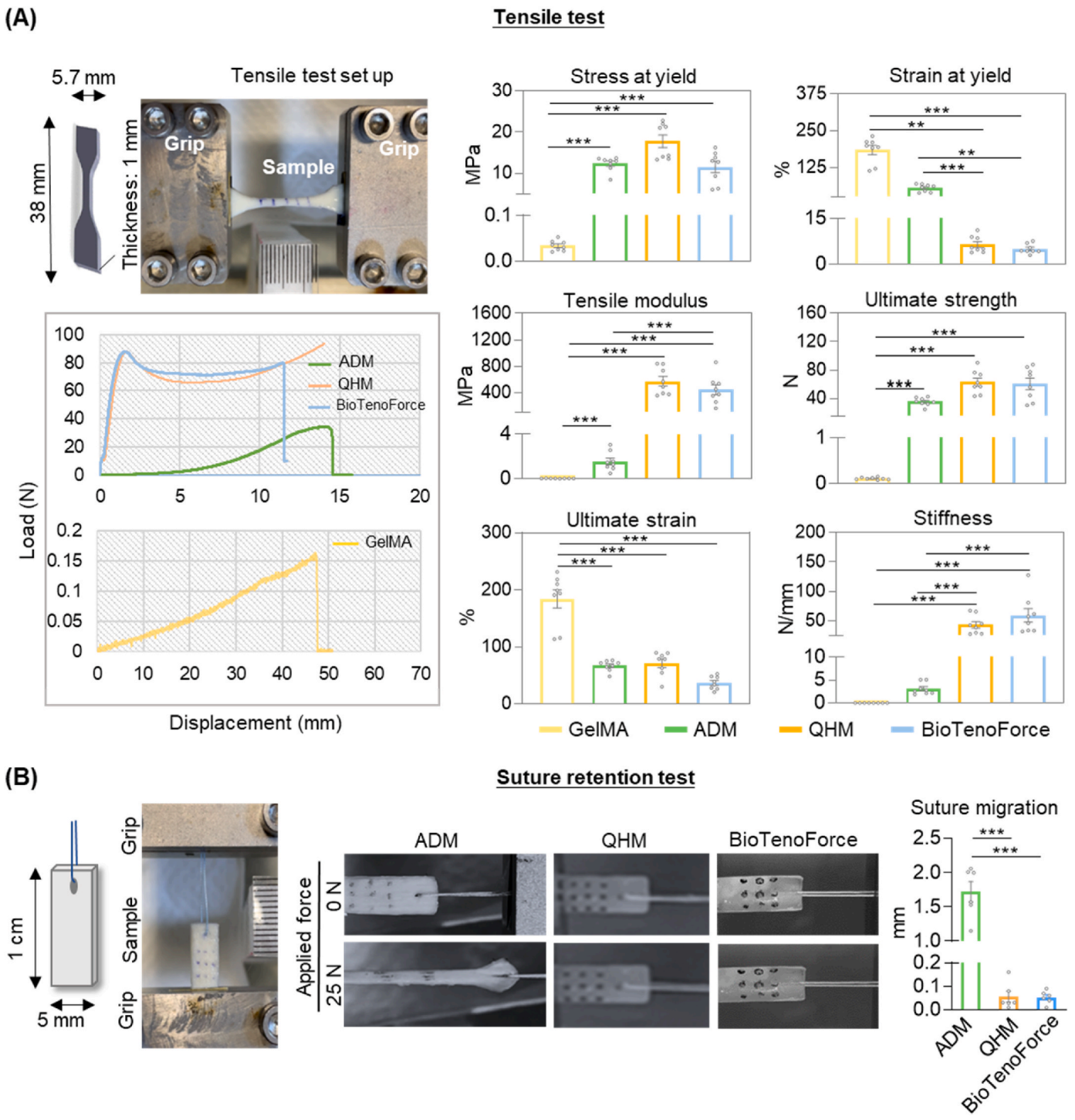

Fig. 2. Tensile properties and suture retention of BioTenoForce. (A) Tensile properties: Schematic illustration of tensile sample dimensions and the tensile test set up in accordance with ASTM standard D638-10. Representative force-displacement graphs and tensile properties demonstrated that QHM elastomer and BioTenoForce exhibited robust tensile attributes, which were superior to ADM (acellular dermal matrix, a leading clinical scaffold control) and GelMA hydrogel. n = 8, technical replicates; mean ± SEM; **, $p < 0.01$; ***, $p < 0.001$. **(B)** Suture retention: Schematic illustration of suture retention sample dimensions and the suture retention test set up. A representative image before (0 N) and during (25 N) suture retention testing and suture migration value suggested that BioTenoForce exhibited superior suture retention properties over ADM. n = 9, technical replicates; mean ± SEM; ***, $p < 0.001$.

inferior gait parameters compared to the uninjured contralateral paw [50]. Our results showed that early after the surgery (day 14), significant differences in gait parameters such as contact area, print width, stride length, and print intensity were observed between the BioTenoForce or defect only group compared to the intact control group (Fig. 4B). However, on days 28 and 56, comparable gait parameters indicating similar gait performance were observed between the BioTenoForce and intact control groups (Fig. 4B). Although some studies have suggested that spontaneous tendon healing can occur in rats [51], the decreased values of contact area, print width, and print intensity and the increased values of swing duration and limb idleness index (LII) indicated that shoulder function was not fully recovered in the defect only group even

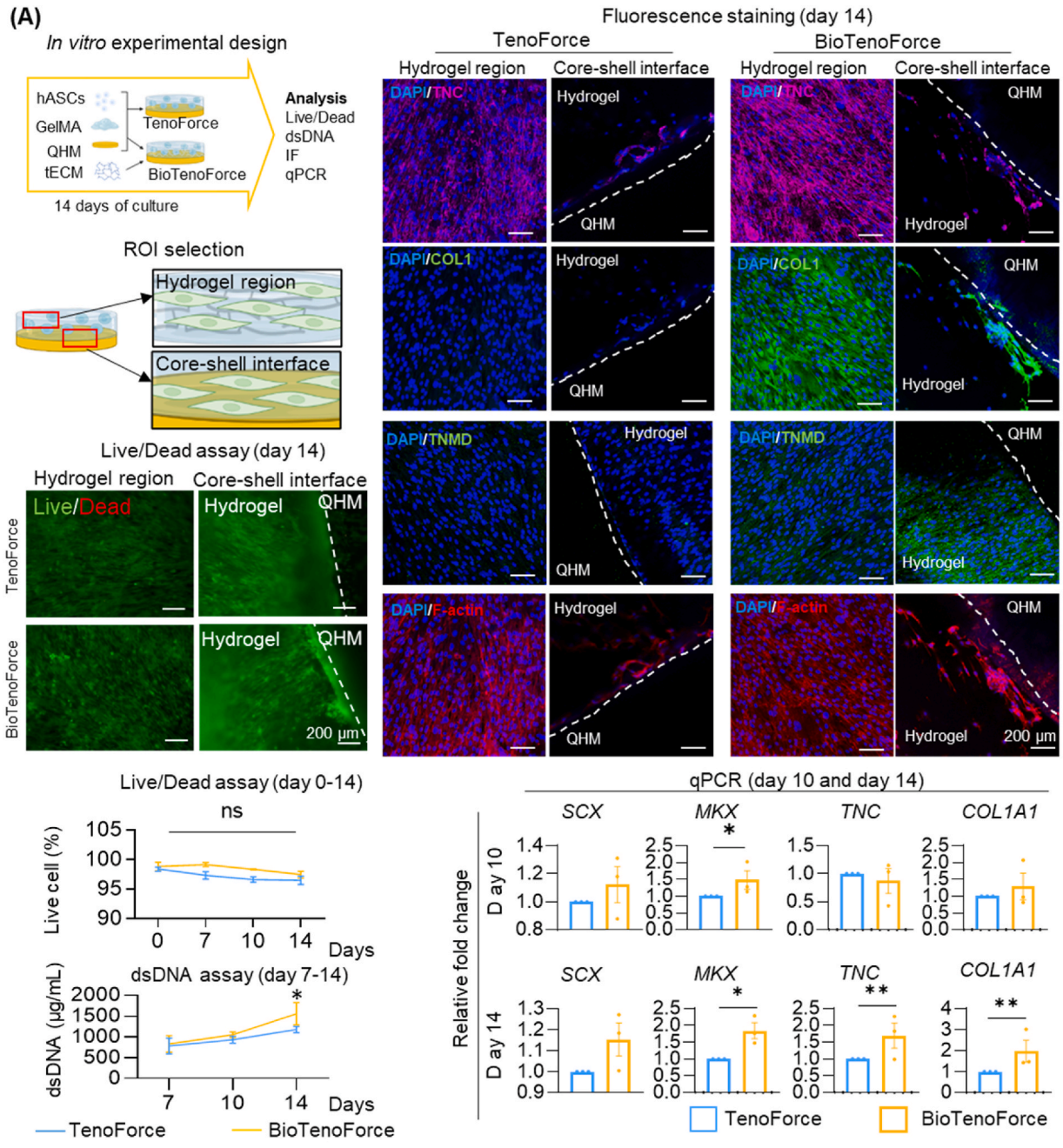

(caption on next page)

Fig. 3. Biocompatibility and tenogenic bioactivity of BioTenoForce. (A) *In vitro* study: Viability (Live/Dead assay), proliferation (dsDNA assay), and tenogenic differentiation (gene expression and fluorescence staining of tenogenesis-associated markers (TNC (Tenascin C), COL1 (Type I collagen), TNMD (Tenomodulin)) and cytoskeleton visualization (F-actin)) of hASCs encapsulated in BioTenoForce or the scaffold without tECM supplementation (called TenoForce) were measured. The results showed that both TenoForce and BioTenoForce were cytocompatible, but BioTenoForce markedly promoted hASC proliferation and tenogenic differentiation to TenoForce. n = 3, biological replicates; mean ± SEM; *, $p < 0.05$; **, $p < 0.01$. **(B)** *In vivo* histobiocompatibility study: H&E and immunohistochemical staining of TenoForce and BioTenoForce in a mouse subcutaneous implantation model. At day 7, a few CD11b + cells (a pan-myeloid marker) were observed at the surface area of the BioTenoForce. By day 28, both groups were surrounded by a thin fibrous capsule, and there was no obvious evidence of an overexuberant inflammatory response. The results showed that both TenoForce and BioTenoForce were biocompatible. White dashed lines indicate the scaffold surface. S: scaffold; n = 3, biological replicates.

56 days after surgery (Fig. 4B). Additionally, to evaluate the biomechanical properties of the BioTenoForce-repaired tendon, a tensile test was conducted at 56 days post-surgery (Fig. S7A). The results revealed that there was no significant difference in terms of ultimate load and stiffness between the intact control group and the group repaired with the BioTenoForce scaffolds (Fig. S7B). These findings indicate that the implantation of the BioTenoForce scaffold successfully restores the biomechanical properties of the tendon defect in rats. In summary, using a rat large rotator cuff tendon defect model, our results demonstrated that BioTenoForce promoted early shoulder functional restoration as evidenced by gait analysis.

3.7. BioTenoForce enhanced tendon healing in rabbits with massive rotator cuff tendon defects

The tendon healing efficacious of BioTenoForce was further evaluated in a rabbit massive rotator cuff tendon defect model (Fig. 5A). A 1-cm tendon defect gap was created on rabbit SSPT and implanted with TenoForce or BioTenoForce to completely bridge the tendon defect, and the contralateral shoulder was used as an intact control group. The efficacy of the BioTenoForce was evaluated using multiple assessment strategies, including gross appearance, histological assessment, SEM, nanoindentation, and tensile testing. These techniques allowed for a comprehensive examination of both macroscopic and microscopic aspects of tendon healing.

At 1 month post-surgery, there were no obvious symptoms of severe inflammation in either TenoForce or BioTenoForce groups based on the gross appearance of tendons (Fig. 5B). Histologically, hematoxylin and eosin (H&E) staining images revealed that both defect groups exhibited complete bridging of the 1-cm tendon defect and increased cellularity relative to the intact control group. However, notable differences in the quality of the healing tissue were observed among the groups. Semi-quantitative cellular orientation analysis showed that cells were more aligned in the BioTenoForce groups than in TenoForce group at both 1 and 3 months post-surgery (Fig. 5B). Also, picrosirius red staining and polarized light microscopy (Fig. S8) were employed to assess the birefringent nature of anisotropic ECM molecules, as well as the size of deposited collagen fibers, with the color hue of the images representing the relative collagen fiber thickness (in order of thinnest to thickest: green, yellow, orange, and red). A typical feature of tendon scar tissue is less birefringence [52]. The results showed that the BioTenoForce group had more pronounced birefringence than the TenoForce group. Additionally, BioTenoForce group had more orange-to-red (thicker) fibers, while TenoForce group had more yellow (thinner) fibers (Fig. 5B). Notably, the widely used direct suture method, which represents the most common surgical intervention [53], demonstrated limited efficacy in promoting tendon regeneration and resulted in the formation of scar-like tissue (Fig. S9). Overall, the histological analysis demonstrated that BioTenoForce exhibited enhanced collagen content and better cellular and ECM organization at both 1 and 3 months post-surgery compared to the TenoForce group, which lacked tECM supplementation.

Additionally, we applied multi-scale analysis (SEM, nanoindentation, and tensile testing) with a special focus to capturing the complex changes in thickness and alignment of collagen fibers during tendon healing, as well as the biomechanical properties of the repaired tendon at 3 months post-surgery (Fig. 6A–C). Ultrastructural analysis using SEM showed that fibers in the intact control and the BioTenoForce groups were aligned along the longitudinal direction of the tendons, while fibers were discretely oriented in the TenoForce group. Interestingly, the collagen fibers in the BioTenoForce and TenoForce groups were comparable in diameter and smaller than those in the intact control group (Fig. 6A). The nanoindentation test revealed that the intact control group (138.5 ± 7.6 kPa) exhibited a higher elastic modulus of collagen fibers than that in the BioTenoForce (20.9 ± 1.9 kPa) and TenoForce (23.9 ± 5.5 kPa) groups, while no significant difference was observed between BioTenoForce and TenoForce groups (Fig. 6B). The bulk biomechanical features of regenerated tendon-scaffold constructs were evaluated using tensile test of the intact control group, TenoForce group, BioTenoForce group, and a time-zero repair group (*i.e.*, a mock surgery performed on cadaveric rabbits) (Fig. 6C). In the time-zero repair group, all tendons failed at the tendon mid-substance due to suture pullout. There were no differences in failure mode among the intact control, TenoForce, and BioTenoForce groups (Fig. 6C). The tensile test results showed that the BioTenoForce scaffold group achieved a comparable ultimate load and stiffness with the intact control group. Furthermore, although TenoForce group showed a comparable ultimate load with the intact control and BioTenoForce group, its stiffness was significantly lower than that of BioTenoForce group (Fig. 6C).

We also performed a correlation coefficient analysis to gain a preliminary understanding of the relationship between collagen fiber structure (thickness, alignment by SEM) and the mechanical features of regenerated tendons at microscale (the elastic modulus of collagen fibers measured by the nanoindentation) and macroscale levels (the ultimate load and stiffness measured by tensile test) (Fig. 6D). Our study yielded several key findings: Firstly, we observed a very strong correlation between the elastic modulus of collagen fibers and their thickness ($r = 0.82$, $p = 0.011$). Secondly, we found that the ultimate load of regenerated tendons did not show any correlation with collagen fiber thickness or alignment, suggesting that QHM elastomer played an important role in contributing to the overall mechanical strength of the tendons-scaffold construct; Finally, we noted a very strong correlation between the stiffness of regenerated tendons and collagen fiber alignment ($r = 0.78$, $p = 0.013$).

In summary, our results demonstrated that BioTenoForce enhanced collagen production and fiber alignment (as shown by histology, histomorphometry, and SEM analysis), and stiffness of regenerated tendon comparable to that of the intact control tendons (as shown by tensile test). Neither TenoForce or BioTenoForce exhibited comparable fiber thickness and modulus to the intact control tendon, indicating an early tendon healing phase at 3 months post-surgery. However, no scaffold breakage was observed throughout the experimental duration, highlighting the critical role of sustained mechanical support provided by scaffolds before the tendon completes healing.

4. Discussion

To attain successful tendon repair in cases of large-to-massive tendon defects, we developed a BioTenoForce with a focus on addressing two pivotal factors: sustained mechanical support and enhanced regenerative bioactivity. The tECM hydrogel shell section of the BioTenoForce was employed to provide tendon-specific bioactivity with improved tendon-like ECM alignment, while the QHM core portion was designed

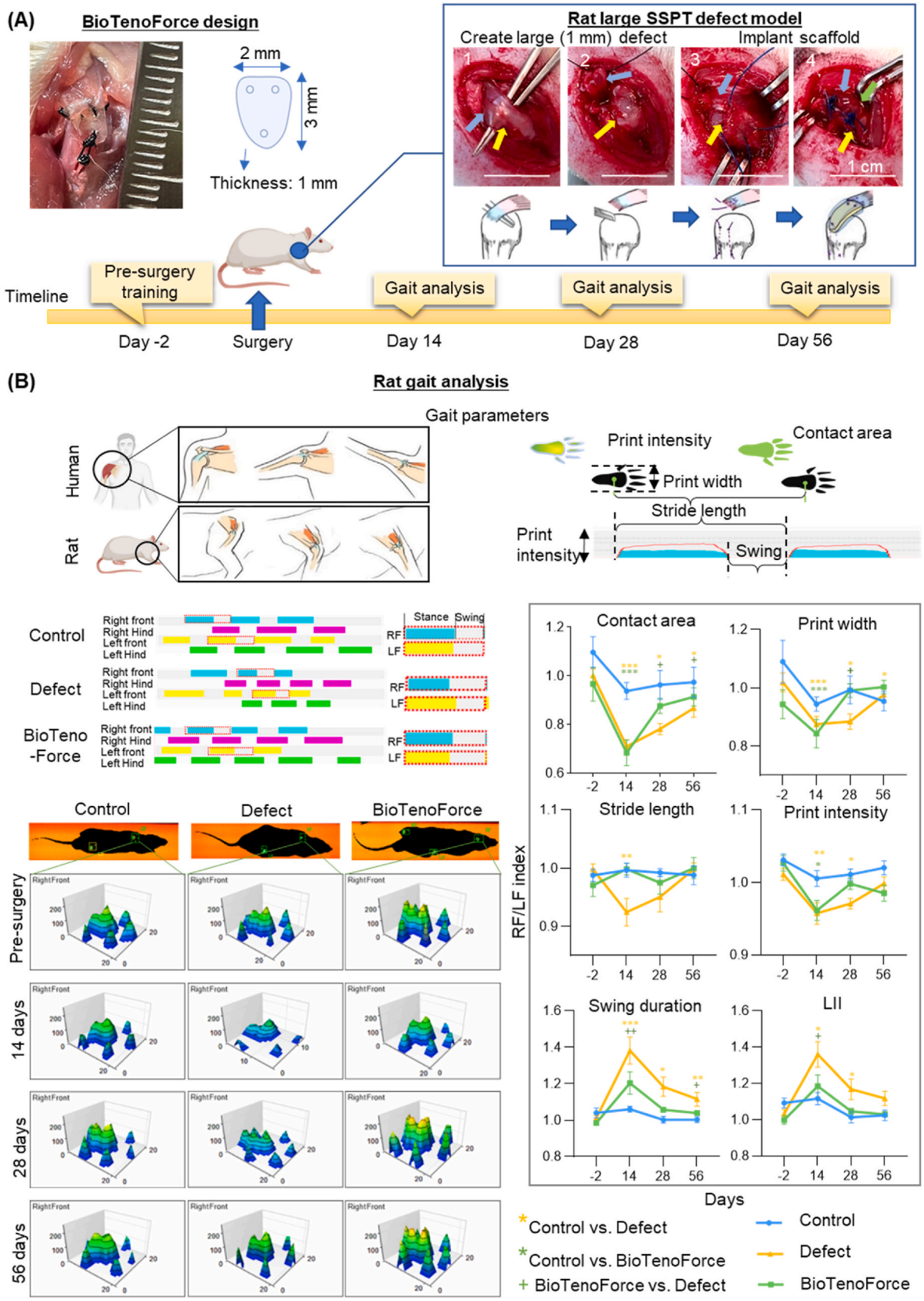

Fig. 4. Gait performance assessment of BioTenoForce-mediate tendon repair in a rat large rotator cuff tendon defect model. (A) Study overview: Schematic illustration and representative macroscopic images of surgical procedures. **(B)** Gait analysis: Gait analysis was performed for 6 parameters (*i.e.*, contact area, print width, stride length, print intensity, swing duration, and LII) of the control, defect only, and BioTenoForce groups at preoperative 2 days and post-surgery 14, 28, and 56 days. Representative paw prints for the right and left front limbs of each group are shown. Similar gait performance was observed in BioTenoForce and intact control group at 28 days post-surgery, but not defect only group, indicating recovered shoulder function in the BioTenoForce group. SSPT: supraspinatus tendon; RF: right forelimb; LF: left forelimb; LII: limb idleness index; n = 10, biological replicates; mean ± SEM; *, $p < 0.05$; **, $p < 0.01$; and ***, $p < 0.001$.

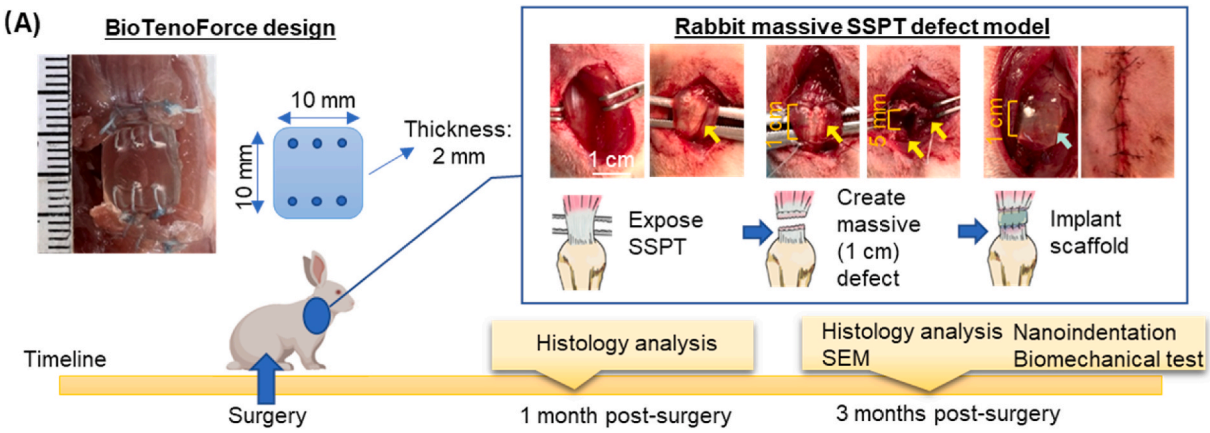

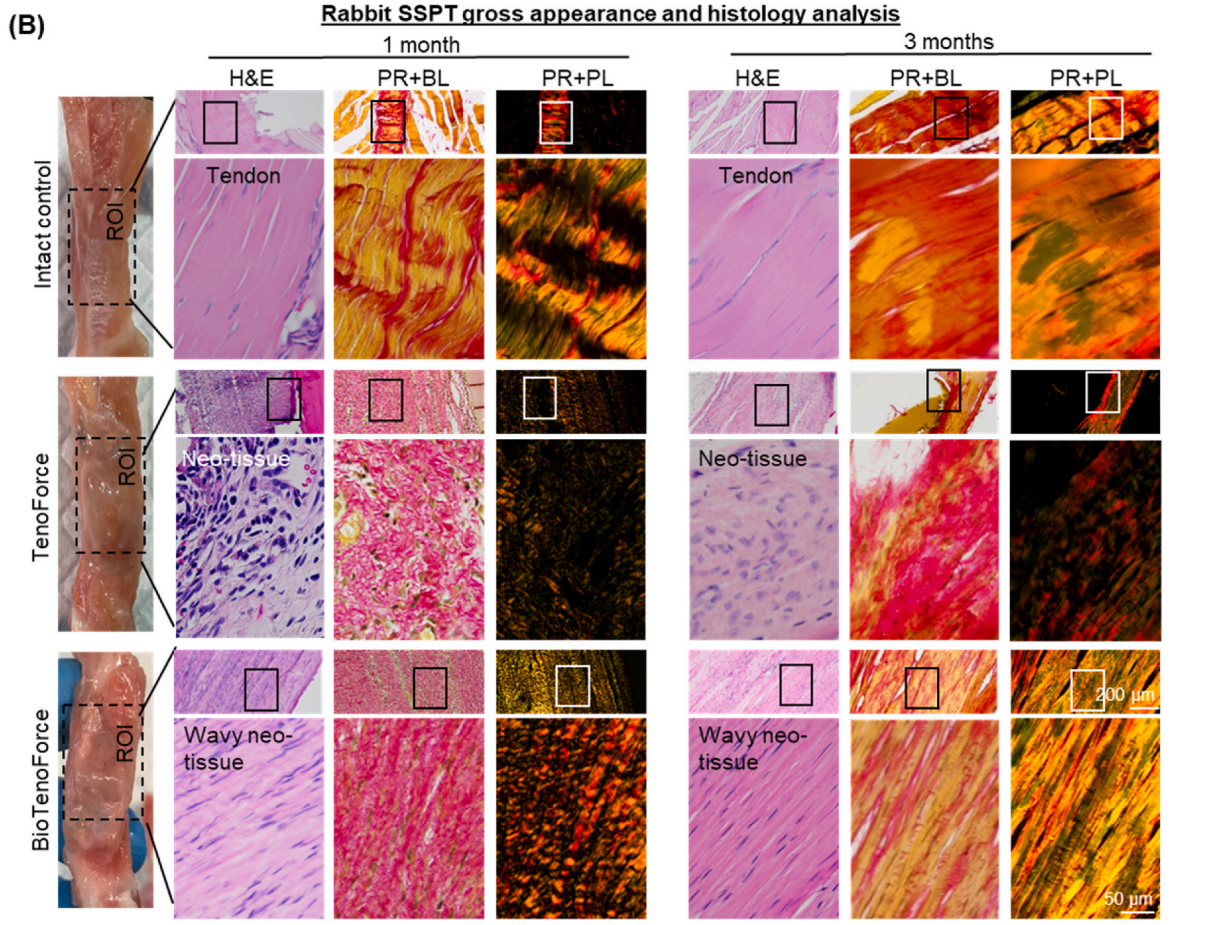

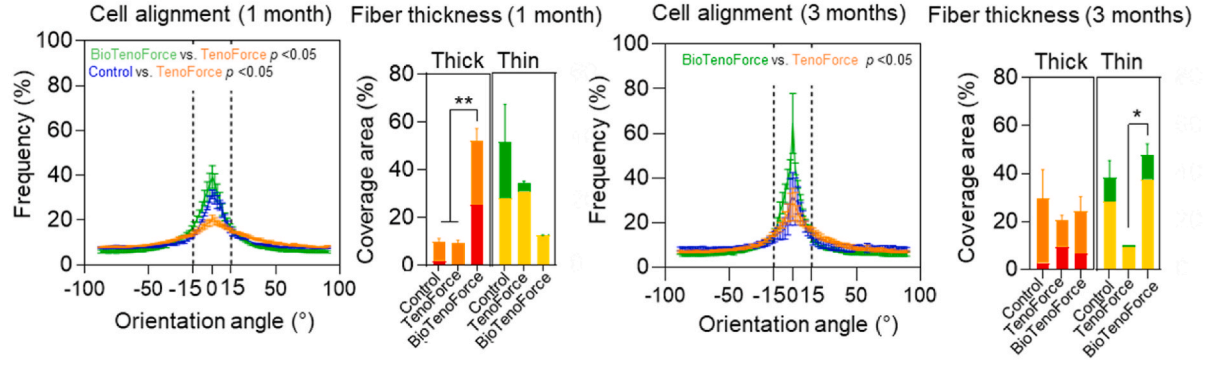

(caption on next page)

Fig. 5. Histological assessment of BioTenoForce for tendon repair in a rabbit massive rotator cuff defect model. (A) Experimental overview and surgical procedure. Yellow arrows indicate tendon, blue arrow indicates implanted scaffolds. **(B)** Gross tissue and histological assessment: At 1 month post-surgery, there were no obvious symptoms of severe inflammation in either TenoForce or BioTenoForce groups based on gross appearance observation. The BioTenoForce group exhibited better cellular alignment than the TenoForce group at both 1 and 3 months. Additionally, the results of picrosirius red staining and polarized light microscopy indicated that the BioTenoForce group demonstrated a wavy, more aligned ECM structure (more pronounced birefringence), with significantly larger number of thicker collagen fibers observed at 1 month and significantly more abundant thinner collagen fibers observed at 3 months compared to the TenoForce group. Overall, the histological analysis revealed that BioTenoForce exhibited enhanced collagen production and superior cellular and ECM organization at both 1 and 3 months post-surgery compared to the TenoForce group. PR: picrosirius red; BL: bright light; PL: polarized light; n = 3, biological replicates; mean ± SEM; *, $p < 0.05$.

to provide long-term mechanical support and durability (Scheme 1).

A main novelty of our study is the combination of two major components: tECM and QHM elastomer *via* benzophenone photocrosslinking in a core-shell strategy to generate BioTenoForce (Schemes 1 and 2). This scaffold design capitalizes on the synergistic effect of combining biological and biomechanical augmentation, thereby offering promising prospects for enhancing tendon repair outcomes. Our tECM component was prepared using a unique urea extraction protocol that is expected to be superior for tendon regeneration [33] compared to traditional acid-pepsin digested ECM lacking substantial non-collagenous tendon proteins [54], or skin-derived ECM products lacking tendon-specific differentiation capability [36,55]. Meanwhile, the QHM elastomer component is expected to approximate human tendon-like biomechanical attributes with excellent suture retention, and slow degradation, to provide sufficient mechanical support during the lengthy tendon healing process, particularly in large-to-massive tendon defects (Scheme 2). Indeed, possessing native tissue-like attributes such as elasticity has been reported to be crucial for efficient musculoskeletal movement while low suture migration and slow degradation are vital for maintaining integrity of the repaired shoulder construct [37,56].

We conduct a comprehensive characterization of the scaffold features including: bonding robustness, mechanical properties, suture retention strength (Figs. 1–2). We modified a previously reported strategy for hydrogel-elastomer bonding [39] and reduced the UV exposure time from 1 h to 90 s. Our data showed that using this revised protocol, our hybrid construct exhibited excellent bonding integrity *ex vivo* and *in vivo* (Fig. 1), and importantly, the benzophenone photocrosslinking procedure did not affect QHM mechanical attributes and suture retention (Fig. 2) or tECM-GelMA *in vitro* bioactivity (Fig. 2). Although some commercial scaffolds (*e.g.*, GraftJacket®) has been widely applied in clinic, their application is limited due to the poor suture retention and insufficient mechanical support [57,58]. Importantly, our BioTenoForce scaffold exhibits tendon-like mechanical properties as well as strong suture retention strength which provides sufficient mechanical properties after implantation.

Our study included a comprehensive preclinical evaluation of tECM for tendon repair including three separate *in vivo* models. *In vivo* assessment is critical because it provides evidence to determine the suitability of BioTenoForce for clinical trials, as well as generate insights to allow us to further scaffold design optimization. Mouse subcutaneous studies showed the viability of our core-shell strategy in maintaining robust hydrogel-elastomer bonding (Fig. 1) as well as BioTenoForce's biocompatibility (Fig. 3). Despite creating a large (1 mm segmental) tendon defect, rat gait performance showed no difference between the BioTenoForce and intact control groups at 1 month after surgery (Fig. 4). Additionally, although some studies have suggested that spontaneous tendon healing is seen in rats [51] our study showed inferior gait performance in the defect group, indicating that shoulder function was not able to attain pre-injury levels even 56 days after surgery (Fig. 4). Consistently, BioTenoForce also achieved enhanced tendon healing in a massive (1 cm) rabbit rotator cuff tendon defect model, as evidenced by improved ECM alignment and biomechanical properties (Figs. 5–6). Together, these findings highlight BioTenoForce efficacy for treatment of large-to-massive tendon injuries.

Generally, early failures of tendon (rotator cuff) repair usually represent an inability of the surgical construct to maintain the mechanical integrity of the repair site, while later tendon repair failures likely signify a biological failure to heal [2]. Collectively, our *in vivo* data highlight the following important findings: (1) There is significant positive contribution of tECM in the BioTenoForce design for tendon repair. Implantation of BioTenoForce, but not TenoForce, led to early and fast tendon fiber alignment (histology and SEM), which was highly correlated with enhanced tendon stiffness (tensile test; Fig. 6). This is crucial because restoring tendon stiffness after injury is required for fulfilling its functional performance [56,59–61]. While many studies have shown that repaired tendon can achieve pre-injury levels in terms of maximum load, achieving native tissue-like stiffness can still be challenging, with several reported values that are an order of magnitude lower than the intact tendon [11,62,63]. (2) The contribution of the elastomer core of the scaffold is also significant and should not be neglected. Tendon healing encompasses a lengthy healing process that takes months and years [64]. Indeed, at 3 months post-surgery, the collagen fiber diameter and modulus (SEM and nanoindentation; Fig. 6) results suggested that the repaired tendons in BioTenoForce and TenoForce groups were still at the early healing phase compared to the intact tendon group. However, we did not observe any breakage or ruptures in our scaffolds, suggesting that before collagen fibers fully mature, the elastomer core with its excellent biomechanical strength, suture retention value, could sufficiently and permanently support the dynamic loading strain during the tendon healing phase and prevent early tendon retear or scaffold failure after surgery. It is worth noting that in a clinical setting, nondegradable devices, including PET patch (nondegradable synthetic graft), suture anchors (*e.g.*, polyether ether ketone; PEEK) and sutures (*e.g.*, high molecular weight polyethylene or FiberWire®), are routinely used and not removed after surgery [23,65,66]. However, even though they can reinforce the mechanical properties, their application is limited due to the poor tenogenic-bioactivity [38]. Tissue ingrowth could prevent micromotion between tissue and implant, avoiding poor biological and mechanical integration between scaffold and neo-tissue that may lead to failed tissue bridging. The incorporation of tECM portion in our graft is intended to enhance intrinsic tissue regeneration capacity and result in a seamless connection between the scaffold with the tendon remnants. Thus, these findings support the use of BioTenoForce *via* a core-shell strategy to simultaneously induce tendon regeneration and achieve adequate mechanical support for efficacious repair of large tendon defects.

There were several limitations in the present study. Firstly, creating a large segmental defect in the rat SSPT posed a considerable challenge. Despite the rat's SSPT having a total length of approximately 16.2 mm [67], the majority of the tendon is embedded within the supraspinatus muscle, resulting in less than 3.5 mm of exposed tendon length [41,68]. Due to the small size of the rat SSPT, our assessment options are limited to employing a bone-to-tendon defect approach to assess the therapeutic effect of the BioTenoForce scaffold. As a result, our evaluation primarily focuses on assessing the functional recovery in the rat model, while a separate rabbit model is utilized to evaluate the outcomes related to structural and biomechanical regeneration. Additionally, our gait analysis was conducted on rats, which are quadruped animals, and may not accurately simulate post-operative joint forces in human patients. Future studies that pair our data with additional investigations in human cadavers to assess joint range of motion will provide stronger evidence of recovery by monitoring for clinically relevant indications such as acromial impingement [69,70]. Secondly, we lack long-term evaluation of mechanical performance of BioTenoForce *in vivo* which is a crucial

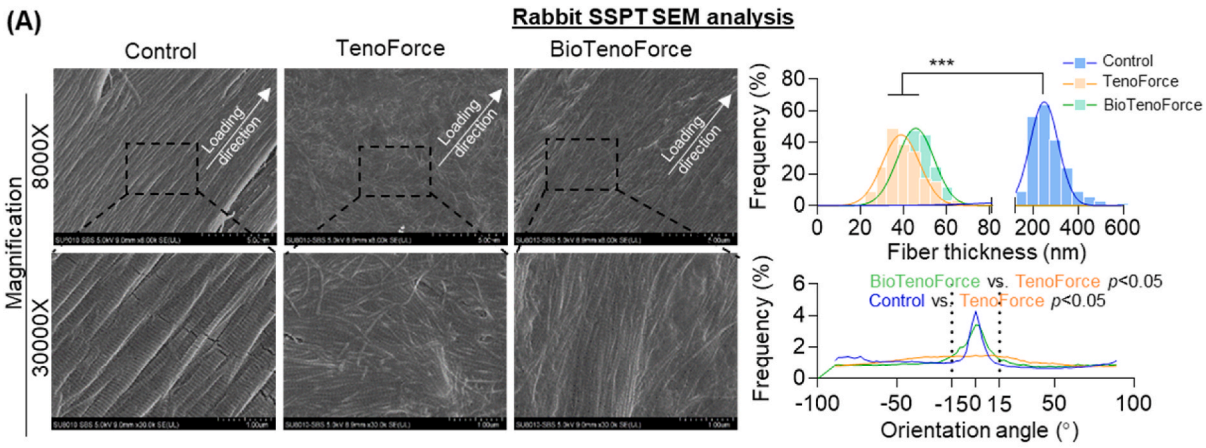

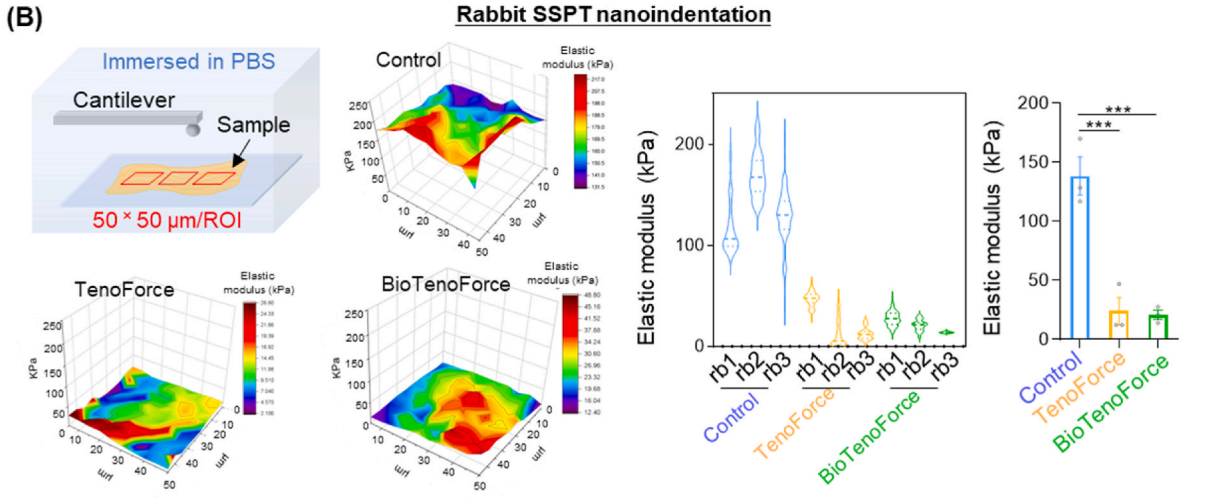

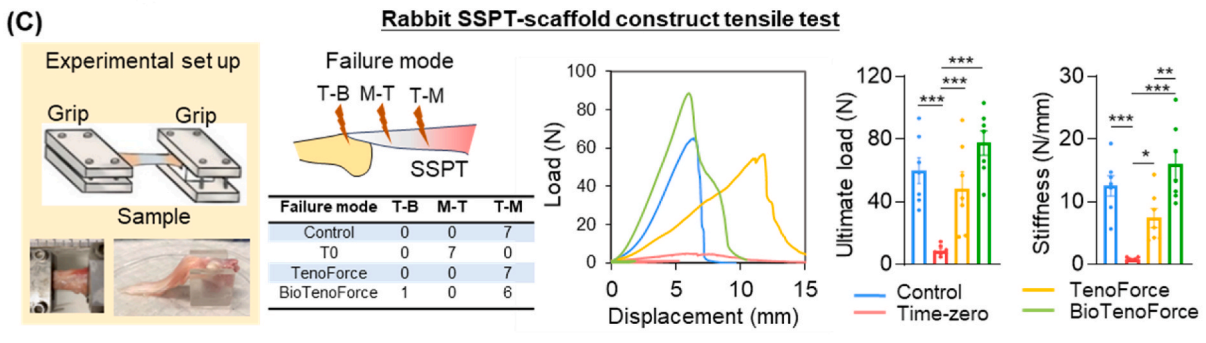

Failure mode	T-B	M-T	T-M
Control	0	0	7
T0	0	7	0
TenoForce	0	0	7
BioTenoForce	1	0	6

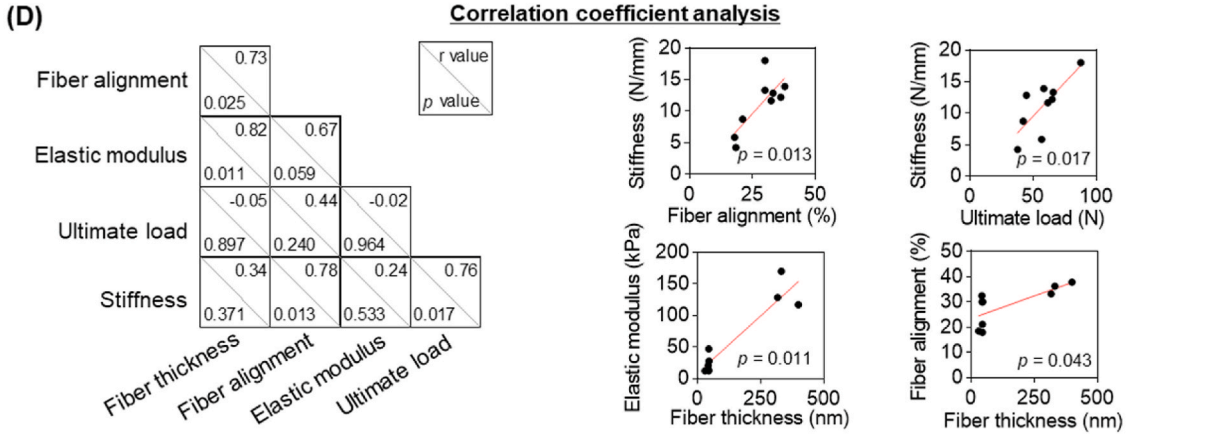

(caption on next page)

Fig. 6. Ultrastructural and bulk biomechanical assessment of BioTenoForce for repairing rabbit massive tendon defects. (A–B) At 3 months after surgery, SEM showed that both BioTenoForce and the intact control groups, but not TenoForce group, exhibited more aligned matrix structure along the longitudinal direction of the tendons. The collagen fibers in both BioTenoForce and TenoForce groups were of comparable size, but exhibited a smaller diameter (SEM) and a lower elastic modulus (nanoindentation) than those in the intact control group. n = 3, biological replicates; mean ± SEM; *, $p < 0.05$. **(C)** Tensile test showed that the TenoForce group had a comparable ultimate load with the intact control and BioTenoForce group, but its stiffness was significantly lower than that of BioTenoForce group. The time-zero repair group (T0): a mock surgery where BioTenoForce were implanted in cadaver rabbits; T–B: tendon to bone junction; M–T: mid-substance of tendon; T–M: tendon to muscle junction; n = 7, biological replicates; mean ± SEM; *, $p < 0.05$; **, $p < 0.01$; and ***, $p < 0.001$. **(D)** Correlation coefficient analysis revealed strong correlation between the elastic modulus and thickness of collagen fibers (r = 0.82, $p = 0.011$). The ultimate load of regenerated tendons did not show any correlation with collagen fiber thickness or alignment, but the stiffness of regenerated tendons showed a very strong correlation with collagen fiber alignment (r = 0.78, $p = 0.013$).

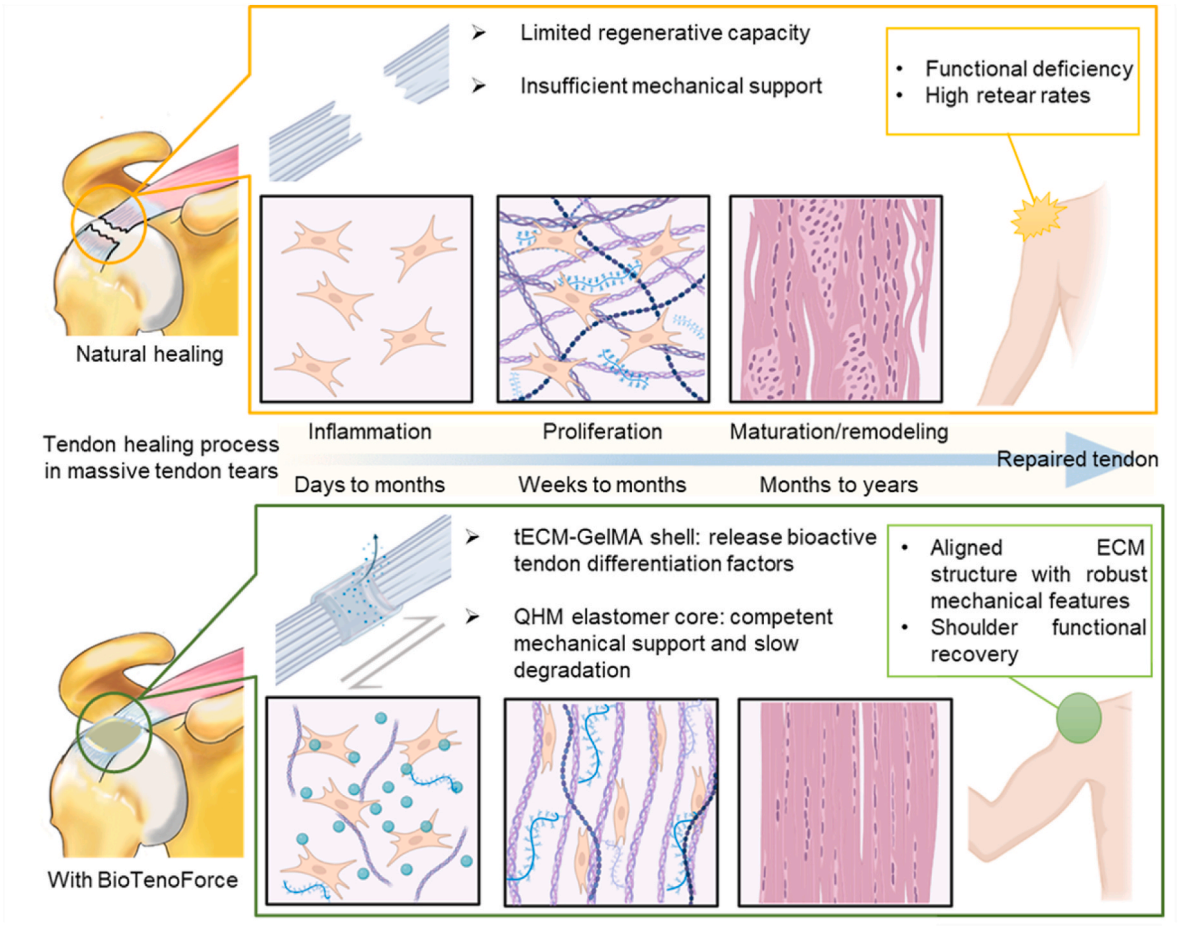

Scheme 2. Mechanistic insights into the role of BioTenoForce in augmenting healing of massive rotator cuff tendon defects. When adult tendons are injured, they typically heal through scar tissue formation with disorganized ECM structure and inferior mechanical features, leading to functional deficiencies. In this study, incorporating a tECM coating onto the BioTenoForce resulted in the regeneration of wavy, well-organized collagen structure. This represents a significant improvement over natural scar tissue formation, as an aligned matrix is a key factor for tendons to sustain strong tensile force. Furthermore, since tendon injury requires a prolonged healing process, the BioTenoForce can provide sufficient, long-term mechanical support to facilitate tendon movement and prevent premature injury before the tendon healing is complete. This activity is particularly crucial in cases of large tendon defects, which have a high prevalence of post-surgery failure. Thus, the BioTenoForce design holds significant promise for promoting tendon regeneration and improving clinical outcomes in cases of large-to-massive tendon defects.

feature for design of nondegradable materials. Despite this, we demonstrated the slow-to-no degradation of QHM elastomer (in NaOH, HCl, H_2O_2, and HBSS) *ex vivo*, estimated to be on the order of several years based on our prior study [37] is ideal for tendon repair, as tendon repairs slowly over months and years. In such a scenario, slow degradation can maintain repair integrity and minimize clinical complications such as loose glenohumeral bodies in the case of rapidly degradable suture anchors and tendon grafts [71]. Thirdly, as our strategy focuses on specifically addressing the repair of large tendon defects, it will become increasingly important to evaluate the healing efficacy of our scaffold in a clinically relevant large animal model. Nevertheless, we believe that the insights and knowledge gained from our study, which utilized two animal models with large tendon defects, can be valuable for our future work as well as for other researchers working with large animal models [72].

5. Conclusion

In conclusion, we have effectively developed a bioactive scaffold that merges two notable technologies: tECM to promote superior tendon regeneration and QHM elastomer for strong mechanical competence and reinforcement. Our results clearly demonstrate that the combination of bioactive factors and mechanical support significantly improves the repair efficacy of large-to-massive tendon defects with BioTenoForce.

We observed a wavy aligned, tendon-like ECM structure, which is vastly different than the typical disorganized scar tissue formation observed after tendon repair. Moreover, the application of BioTenoForce in two challenging large tendon defect animal models provide a comprehensive preclinical evaluation. Remarkably, we did not observe any scaffold damage during the entire experiment, and regenerated tendons exhibited native tendon-like robust mechanical features indicating the great potential of BioTenoForce for clinical translation (Scheme 2). Therefore, our findings represent a major and significant advance in the field of tendon tissue engineering and offer a promising new approach to clinical tendon repair, especially in the scenarios involving large tendon defects. Furthermore, we believe that our simple, yet versatile hybrid construct design will open new avenues for practical applications of using our urea-based ECM technology with other biomaterial scaffolds in diverse areas for robust tissue regeneration.

Ethics approval and consent to participate

The hASC isolation was conducted according to the guidelines of the Institutional Review Board (IRB). Informed consent was obtained from all subjects involved in the study. The *in vivo* studies were conducted according to the institution's Animal Experimentation Ethics Committee (AEEC).

Declaration of competing interest

Dr. Dan Wang is an editorial board member for Bioactive Materials and was not involved in the editorial review or the decision to publish this article. All authors declare that there are no competing interests.

CRediT authorship contribution statement

Shuting Huang: Writing – review & editing, Writing – original draft, Visualization, Validation, Methodology, Investigation, Formal analysis, Data curation. **Ying Rao:** Writing – review & editing, Writing – original draft, Methodology, Investigation, Formal analysis. **Meng Zhou:** Methodology, Investigation. **Anna M. Blocki:** Writing – review & editing, Funding acquisition. **Xiao Chen:** Writing – review & editing. **Chunyi Wen:** Writing – review & editing, Methodology, Formal analysis. **Dai Fei Elmer Ker:** Writing – review & editing, Funding acquisition, Conceptualization. **Rocky S. Tuan:** Writing – review & editing, Supervision, Project administration, Investigation, Funding acquisition, Conceptualization. **Dan Michelle Wang:** Writing – review & editing, Supervision, Project administration, Investigation, Funding acquisition, Formal analysis, Conceptualization.

Acknowledgements

We express our gratitude to all donors, study coordinators, administrators, and laboratory managers involved in this work. We express our gratitude to the funding support, including The Research Grants Council of Hong Kong SAR (GRF 14121121, DMW; GRF 14118620, DMW; ECS24201720, DFEK), National Natural Science Foundation of China/Research Grants Council Joint Research Scheme (N_CUHK409/23, DMW), and The Innovation and Technology Commission of Hong Kong SAR Innovation Tier 3 Support (ITS/090/18, DFEK) and Health@InnoHK CNRM (DMW, AB, DFEK, RST).

Appendix B. Supplementary data

Supplementary data to this article can be found online at https://doi.org/10.1016/j.bioactmat.2024.02.032.

References

[1] J.H. Wang, Q. Guo, B. Li, Tendon biomechanics and mechanobiology–a minireview of basic concepts and recent advancements, J. Hand Ther. 25 (2) (2012) 133, 140; quiz 141.
[2] F.A. Matsen 3rd, Clinical practice. Rotator-cuff failure, N. Engl. J. Med. 358 (20) (2008) 2138–2147.
[3] G.B.D. Disease, I. Injury C, Prevalence, Global, regional, and national incidence, prevalence, and years lived with disability for 328 diseases and injuries for 195 countries, 1990-2016: a systematic analysis for the Global Burden of Disease Study 2016, Lancet 390 (10100) (2017) 1211–1259.
[4] L.M. Galatz, C.M. Ball, S.A. Teefey, W.D. Middleton, K. Yamaguchi, The outcome and repair integrity of completely arthroscopically repaired large and massive rotator cuff tears, J Bone Joint Surg Am 86 (2) (2004) 219–224.
[5] S.J. Kim, S.H. Kim, S.K. Lee, J.W. Seo, Y.M. Chun, Arthroscopic repair of massive contracted rotator cuff tears: aggressive release with anterior and posterior interval slides do not improve cuff healing and integrity, J Bone Joint Surg Am 95 (16) (2013) 1482–1488.
[6] L.M. Galatz, L. Gerstenfeld, E. Heber-Katz, S.A. Rodeo, Tendon regeneration and scar formation: the concept of scarless healing, J. Orthop. Res. 33 (6) (2015) 823–831.
[7] J.M. Geremia, M.F. Bobbert, M. Casa Nova, R.D. Ott, A. Lemos Fde, O. Lupion Rde, V.B. Frasson, M.A. Vaz, The structural and mechanical properties of the Achilles tendon 2 years after surgical repair, Clin. Biomech. 30 (5) (2015) 485–492.
[8] S. Font Tellado, E.R. Balmayor, M. Van Griensven, Strategies to engineer tendon/ligament-to-bone interface: biomaterials, cells and growth factors, Adv. Drug Deliv. Rev. 94 (2015) 126–140.
[9] M.K. Demange, A.M. de Almeida, S.A. Rodeo, Updates in biological therapies for knee injuries: tendons, Curr Rev Musculoskelet Med 7 (3) (2014) 239–246.
[10] B.R. Freedman, D.J. Mooney, E. Weber, Advances toward transformative therapies for tendon diseases, Sci. Transl. Med. 14 (661) (2022) eabl8814.
[11] D.L. Butler, N. Juncosa-Melvin, G.P. Boivin, M.T. Galloway, J.T. Shearn, C. Gooch, H. Awad, Functional tissue engineering for tendon repair: a multidisciplinary strategy using mesenchymal stem cells, bioscaffolds, and mechanical stimulation, J. Orthop. Res. 26 (1) (2008) 1–9.
[12] D. Docheva, S.A. Müller, M. Majewski, C.H. Evans, Biologics for tendon repair, Adv. Drug Deliv. Rev. 84 (2015) 222–239.
[13] S.P. Lake, K.S. Miller, D.M. Elliott, L.J. Soslowsky, Effect of fiber distribution and realignment on the nonlinear and inhomogeneous mechanical properties of human supraspinatus tendon under longitudinal tensile loading, J. Orthop. Res. 27 (12) (2009) 1596–1602.
[14] K.A. Derwin, S.F. Badylak, S.P. Steinmann, J.P. Iannotti, Extracellular matrix scaffold devices for rotator cuff repair, J. Shoulder Elbow Surg. 19 (3) (2010) 467–476.
[15] T. Molloy, Y. Wang, G. Murrell, The roles of growth factors in tendon and ligament healing, Sports Med. 33 (5) (2003) 381–394.
[16] J.K. Mouw, G. Ou, V.M. Weaver, Extracellular matrix assembly: a multiscale deconstruction, Nat. Rev. Mol. Cell Biol. 15 (12) (2014) 771–785.
[17] A.E. Jakus, M.M. Laronda, A.S. Rashedi, C.M. Robinson, C. Lee, S.W. Jordan, K. E. Orwig, T.K. Woodruff, R.N. Shah, "Tissue papers" from organ-specific decellularized extracellular matrices, Adv. Funct. Mater. 27 (3) (2017).
[18] K.A. Derwin, A.R. Baker, R.K. Spragg, D.R. Leigh, J.P. Iannotti, Commercial extracellular matrix scaffolds for rotator cuff tendon repair. Biomechanical, biochemical, and cellular properties, J Bone Joint Surg Am 88 (12) (2006) 2665–2672.
[19] J. Chen, J. Xu, A. Wang, M. Zheng, Scaffolds for tendon and ligament repair: review of the efficacy of commercial products, Expet Rev. Med. Dev. 6 (1) (2009) 61–73.
[20] C.W. Cheng, L.D. Solorio, E. Alsberg, Decellularized tissue and cell-derived extracellular matrices as scaffolds for orthopaedic tissue engineering, Biotechnol. Adv. 32 (2) (2014) 462–484.
[21] H. Zhang, M.F. Liu, R.C. Liu, W.L. Shen, Z. Yin, X. Chen, Physical microenvironment-based inducible scaffold for stem cell differentiation and tendon regeneration, Tissue Eng Part B Rev 24 (6) (2018) 443–453.
[22] B. Shiroud Heidari, E. Muinos Lopez, E. Harrington, R. Ruan, P. Chen, S. M. Davachi, B. Allardyce, R. Rajkhowa, R. Dilley, F. Granero-Molto, E.M. De-Juan-Pardo, M. Zheng, B. Doyle, Novel hybrid biocomposites for tendon grafts: the addition of silk to polydioxanone and poly(lactide-co-caprolactone) enhances material properties, in vitro and in vivo biocompatibility, Bioact. Mater. 25 (2023) 291–306.
[23] Y. Zhong, W. Jin, H. Gao, L. Sun, P. Wang, J. Zhang, M.T.Y. Ong, F. Sai Chuen Bruma, S. Chen, J. Chen, A knitted PET patch enhances the maturation of regenerated tendons in bridging reconstruction of massive rotator cuff tears in a rabbit model, Am. J. Sports Med. 51 (4) (2023) 901–911.
[24] Y.J. No, M. Castilho, Y. Ramaswamy, H. Zreiqat, Role of biomaterials and controlled architecture on tendon/ligament repair and regeneration, Adv. Mater. 32 (18) (2020) e1904511.
[25] L.C. Mozdzen, R. Rodgers, J.M. Banks, R.C. Bailey, B.A. Harley, Increasing the strength and bioactivity of collagen scaffolds using customizable arrays of 3D-printed polymer fibers, Acta Biomater. 33 (2016) 25–33.
[26] A. Islam, M.S. Bohl, A.G. Tsai, M. Younesi, R. Gillespie, O. Akkus, Biomechanical evaluation of a novel suturing scheme for grafting load-bearing collagen scaffolds for rotator cuff repair, Clin. Biomech. 30 (7) (2015) 669–675.
[27] C.C. Tai, C.C. Huang, B.H. Chou, C.Y. Chen, S.Y. Chen, Y.H. Huang, J.S. Sun, Y. H. Chao, Profiled polyethylene terephthalate filaments that incorporate collagen and calcium phosphate enhance ligamentisation and bone formation, Eur. Cell. Mater. 43 (2022) 252–266.

[28] T. Matsuhashi, A.W. Hooke, K.D. Zhao, A. Goto, J.W. Sperling, S.P. Steinmann, K. N. An, Tensile properties of a morphologically split supraspinatus tendon, Clin. Anat. 27 (5) (2014) 702–706.
[29] A. Ratcliffe, D.L. Butler, N.A. Dyment, P.J. Cagle, C.S. Proctor, S.S. Ratcliffe, E. L. Flatow, Scaffolds for tendon and ligament repair and regeneration, Ann. Biomed. Eng. 43 (3) (2015) 819–831.
[30] G. Yang, B.B. Rothrauff, H. Lin, R. Gottardi, P.G. Alexander, R.S. Tuan, Enhancement of tenogenic differentiation of human adipose stem cells by tendon-derived extracellular matrix, Biomaterials 34 (37) (2013) 9295–9306.
[31] D. Wang, C.C.M. Pun, S. Huang, T.C.M. Tang, K.K.W. Ho, B.B. Rothrauff, P.S. H. Yung, A.M. Blocki, E.D.F. Ker, R.S. Tuan, Tendon-derived extracellular matrix induces mesenchymal stem cell tenogenesis via an integrin/transforming growth factor-beta crosstalk-mediated mechanism, Faseb. J. 34 (6) (2020) 8172–8186.
[32] Y. Rao, C. Zhu, H.C. Suen, S. Huang, J. Liao, D.F.E. Ker, R.S. Tuan, D. Wang, Tenogenic induction of human adipose-derived stem cells by soluble tendon extracellular matrix: composition and transcriptomic analyses, Stem Cell Res. Ther. 13 (1) (2022) 380.
[33] B.B. Rothrauff, G. Yang, R.S. Tuan, Tissue-specific bioactivity of soluble tendon-derived and cartilage-derived extracellular matrices on adult mesenchymal stem cells, Stem Cell Res. Ther. 8 (1) (2017) 133.
[34] J. Hackethal, P. Dungel, A.H. Teuschl, Frequently used strategies to isolate extracellular matrix proteins from human placenta and adipose tissue, Tissue Eng. C Methods 27 (12) (2021) 649–660.
[35] X. Xu, L. Zheng, Q. Yuan, G. Zhen, J.L. Crane, X. Zhou, X. Cao, Transforming growth factor-beta in stem cells and tissue homeostasis, Bone Res 6 (2018) 2.
[36] J.A. Soler, S. Gidwani, M.J. Curtis, Early complications from the use of porcine dermal collagen implants (Permacol) as bridging constructs in the repair of massive rotator cuff tears. A report of 4 cases, Acta Orthop. Belg. 73 (4) (2007) 432–436.
[37] D.F.E. Ker, D. Wang, A.W. Behn, E.T.H. Wang, X. Zhang, B.Y. Zhou, A.E. Mercado-Pagan, S. Kim, J. Kleimeyer, B. Gharaibeh, Y. Shanjani, D. Nelson, M. Safran, E. Cheung, P. Campbell, Y.P. Yang, Functionally graded, bone- and tendon-like polyurethane for rotator cuff repair, Adv. Funct. Mater. 28 (20) (2018).
[38] H. Li, J. Li, J. Jiang, F. Lv, J. Chang, S. Chen, C. Wu, An osteogenesis/angiogenesis-stimulation artificial ligament for anterior cruciate ligament reconstruction, Acta Biomater. 54 (2017) 399–410.
[39] H. Yuk, T. Zhang, G.A. Parada, X. Liu, X. Zhao, Skin-inspired hydrogel-elastomer hybrids with robust interfaces and functional microstructures, Nat. Commun. 7 (2016) 12028.
[40] Y. Liu, S.C. Fu, H.T. Leong, S.K. Ling, J.H. Oh, P.S. Yung, Evaluation of animal models and methods for assessing shoulder function after rotator cuff tear: a systematic review, J Orthop Translat 26 (2021) 31–38.
[41] S. Thomopoulos, L.J. Soslowsky, C.L. Flanagan, S. Tun, C.C. Keefer, J. Mastaw, J. E. Carpenter, The effect of fibrin clot on healing rat supraspinatus tendon defects, J. Shoulder Elbow Surg. 11 (3) (2002) 239–247.
[42] J.H. Yea, T.S. Bae, B.J. Kim, Y.W. Cho, C.H. Jo, Regeneration of the rotator cuff tendon-to-bone interface using umbilical cord-derived mesenchymal stem cells and gradient extracellular matrix scaffolds from adipose tissue in a rat model, Acta Biomater. 114 (2020) 104–116.
[43] N. Bhalerao, S. Pagdal, A modified Mason-Allen technique for mini open transosseous rotator cuff repair, International Journal of Orthopaedics 5 (4) (2019) 13–15.
[44] H.M. Klinger, H. Steckel, G. Spahn, G.H. Buchhorn, M.H. Baums, Biomechanical comparison of double-loaded suture anchors using arthroscopic Mason-Allen stitches versus traditional transosseous suture technique and modified Mason-Allen stitches for rotator cuff repair, Clin. Biomech. 22 (1) (2007) 106–111.
[45] C. Gerber, A.G. Schneeberger, M. Beck, U. Schlegel, Mechanical strength of repairs of the rotator cuff, J Bone Joint Surg Br 76 (3) (1994) 371–380.
[46] S.C. Fu, Y.C. Cheuk, L.K. Hung, K.M. Chan, Limb Idleness Index (LII): a novel measurement of pain in a rat model of osteoarthritis, Osteoarthritis Cartilage 20 (11) (2012) 1409–1416.
[47] Z. Zheng, J. Ran, W. Chen, Y. Hu, T. Zhu, X. Chen, Z. Yin, B.C. Heng, G. Feng, H. Le, C. Tang, J. Huang, Y. Chen, Y. Zhou, P. Dominique, W. Shen, H.W. Ouyang, Alignment of collagen fiber in knitted silk scaffold for functional massive rotator cuff repair, Acta Biomater. 51 (2017) 317–329.
[48] T. Moriya, C. Zhao, K.N. An, P.C. Amadio, The effect of epitendinous suture technique on gliding resistance during cyclic motion after flexor tendon repair: a cadaveric study, J Hand Surg Am 35 (4) (2010) 552–558.
[49] A.G. Asuero, A. Sayago, A. González, The correlation coefficient: an overview, Crit. Rev. Anal. Chem. 36 (1) (2006) 41–59.
[50] Y. Xu, N.X. Tian, Q.Y. Bai, Q. Chen, X.H. Sun, Y. Wang, Gait assessment of pain and analgesics: comparison of the DigiGait and CatWalk gait imaging systems, Neurosci. Bull. 35 (3) (2019) 401–418.
[51] J.A. Gimbel, J.P. Van Kleunen, S. Mehta, S.M. Perry, G.R. Williams, L.J. Soslowsky, Supraspinatus tendon organizational and mechanical properties in a chronic rotator cuff tear animal model, J. Biomech. 37 (5) (2004) 739–749.
[52] P. Whittaker, R.A. Kloner, D.R. Boughner, J.G. Pickering, Quantitative assessment of myocardial collagen with picrosirius red staining and circularly polarized light, Basic Res. Cardiol. 89 (5) (1994) 397–410.
[53] F. Oliva, E. Marsilio, F. Migliorini, N. Maffulli, Complex ruptures of the quadriceps tendon: a systematic review of surgical procedures and outcomes, J. Orthop. Surg. Res. 16 (1) (2021) 547.
[54] Z. Fu, S. Akula, M. Thorpe, L. Hellman, Marked difference in efficiency of the digestive enzymes pepsin, trypsin, chymotrypsin, and pancreatic elastase to cleave tightly folded proteins, Biol. Chem. 402 (7) (2021) 861–867.
[55] Z. Yin, X. Chen, T. Zhu, J.J. Hu, H.X. Song, W.L. Shen, L.Y. Jiang, B.C. Heng, J.F. Ji, H.W. Ouyang, The effect of decellularized matrices on human tendon stem/progenitor cell differentiation and tendon repair, Acta Biomater. 9 (12) (2013) 9317–9329.
[56] G.A. Lichtwark, A.M. Wilson, Is Achilles tendon compliance optimised for maximum muscle efficiency during locomotion? J. Biomech. 40 (8) (2007) 1768–1775.
[57] S. Chaudhury, C. Holland, M.S. Thompson, F. Vollrath, A.J. Carr, Tensile and shear mechanical properties of rotator cuff repair patches, J. Shoulder Elbow Surg. 21 (9) (2012) 1168–1176.
[58] N.L. Leong, F.A. Petrigliano, D.R. McAllister, Current tissue engineering strategies in anterior cruciate ligament reconstruction, J. Biomed. Mater. Res. 102 (5) (2014) 1614–1624.
[59] Y. Itoigawa, T. Wada, T. Kawasaki, D. Morikawa, Y. Maruyama, K. Kaneko, Supraspinatus muscle and tendon stiffness changes after arthroscopic rotator cuff repair: a shear wave elastography assessment, J. Orthop. Res. 38 (1) (2020) 219–227.
[60] C.F. Guimarães, L. Gasperini, A.P. Marques, R.L. Reis, The stiffness of living tissues and its implications for tissue engineering, Nat. Rev. Mater. 5 (5) (2020) 351–370.
[61] M. Younesi, A. Islam, V. Kishore, J.M. Anderson, O. Akkus, Tenogenic induction of human MSCs by anisotropically aligned collagen biotextiles, Adv. Funct. Mater. 24 (36) (2014) 5762–5770.
[62] R.F. Henn 3rd, C.E. Kuo, M.W. Kessler, P. Razzano, D.P. Grande, S.W. Wolfe, Augmentation of zone II flexor tendon repair using growth differentiation factor 5 in a rabbit model, J Hand Surg Am 35 (11) (2010) 1825–1832.
[63] L. Wang, Y. Kang, H. Yan, X. Zhu, T. Zhu, J. Jiang, J. Zhao, Tendon regeneration induced by umbilical cord graft in a rabbit tendon defect model, J Tissue Eng Regen Med 14 (8) (2020) 1009–1018.
[64] A.E.C. Nichols, K.T. Best, A.E. Loiselle, The cellular basis of fibrotic tendon healing: challenges and opportunities, Transl. Res. 209 (2019) 156–168.
[65] A.K. Koganti, G.J. Adamson, C.S. Gregersen, M.M. Pink, J.A. Shankwiler, Biomechanical comparison of traditional and locked suture configurations for arthroscopic repairs of the rotator cuff, Am. J. Sports Med. 34 (11) (2006) 1832–1838.
[66] D. Pokorny, P. Fulin, M. Slouf, D. Jahoda, I. Landor, A. Sosna, Polyetheretherketone (PEEK). Part II: application in clinical practice, Acta Chir. Orthop. Traumatol. Cech. 77 (6) (2010) 470–478.
[67] A.P. Valencia, S.R. Iyer, S.J.P. Pratt, M.N. Gilotra, R.M. Lovering, A method to test contractility of the supraspinatus muscle in mouse, rat, and rabbit, J. Appl. Physiol. 120 (3) (2016) 310–317, 1985.
[68] Y. Sun, H.W. Jung, J.M. Kwak, J. Tan, Z. Wang, I.H. Jeon, Reconstruction of large chronic rotator cuff tear can benefit from the bone-tendon composite autograft to restore the native bone-tendon interface, J Orthop Translat 24 (2020) 175–182.
[69] S. Namdari, G. Yagnik, D.D. Ebaugh, S. Nagda, M.L. Ramsey, G.R. Williams Jr., S. Mehta, Defining functional shoulder range of motion for activities of daily living, J. Shoulder Elbow Surg. 21 (9) (2012) 1177–1183.
[70] T.S. Ellenbecker, A. Cools, Rehabilitation of shoulder impingement syndrome and rotator cuff injuries: an evidence-based review, Br. J. Sports Med. 44 (5) (2010) 319–327.
[71] F.A. Barber, Biodegradable shoulder anchors have unique modes of failure, Arthroscopy 23 (3) (2007) 316–320.
[72] D. Little, P.C. Amadio, H.A. Awad, S.G. Cone, N.A. Dyment, M.B. Fisher, A. H. Huang, D.W. Koch, A.F. Kuntz, R. Madi, K. McGilvray, L.V. Schnabel, S. S. Shetye, S. Thomopoulos, C. Zhao, L.J. Soslowsky, Preclinical tendon and ligament models: beyond the 3Rs (replacement, reduction, and refinement) to 5W1H (why, who, what, where, when, how), J. Orthop. Res. 41 (10) (2023) 2133–2162.